Cellular/Molecular

Importin-β11 Regulates Synaptic Phosphorylated Mothers Against Decapentaplegic, and Thereby Influences Synaptic Development and Function at the *Drosophila* Neuromuscular Junction

Misao E. Higashi-Kovtun,[1,2] Timothy J. Mosca,[1,2] Dion K. Dickman,[1,2] Ian A. Meinertzhagen,[3] and Thomas L. Schwarz[1,2]

[1]F. M. Kirby Center for Neurobiology, Children's Hospital, Boston, Massachusetts 02115, [2]Department of Neurobiology, Harvard Medical School, Boston, Massachusetts 02115, and [3]Department of Psychology, Life Sciences Centre, Dalhousie University, Halifax, Nova Scotia B3H 4J1, Canada

Importin proteins act both at the nuclear pore to promote substrate entry and in the cytosol during signal trafficking. Here, we describe mutations in the *Drosophila* gene *importin-β11*, which has not previously been analyzed genetically. Mutants of *importin-β11* died as late pupae from neuronal defects, and neuronal importin-β11 was present not only at nuclear pores but also in the cytosol and at synapses. Neurons lacking importin-β11 were viable and properly differentiated but exhibited discrete defects. Synaptic transmission was defective in adult photoreceptors and at larval neuromuscular junctions (NMJs). Mutant photoreceptor axons formed grossly normal projections and synaptic terminals in the brain, but synaptic arbors on larval muscles were smaller while still containing appropriate synaptic components. Bone morphogenic protein (BMP) signaling was the apparent cause of the observed NMJ defects. *Importin-β11* interacted genetically with the BMP pathway, and at mutant synaptic boutons, a key component of this pathway, phosphorylated mothers against decapentaplegic (pMAD), was reduced. Neuronal expression of an *importin-β11* transgene rescued this phenotype as well as the other observed neuromuscular phenotypes. Despite the loss of synaptic pMAD, pMAD persisted in motor neuron nuclei, suggesting a specific impairment in the local function of pMAD. Restoring levels of pMAD to mutant terminals via expression of constitutively active type I BMP receptors or by reducing retrograde transport in motor neurons also restored synaptic strength and morphology. Thus, importin-β11 function interacts with the BMP pathway to regulate a pool of pMAD that must be present at the presynapse for its proper development and function.

Introduction

The complex and dynamic nature of neuronal circuits necessitates well-orchestrated signals to direct the development, maintenance, and plasticity of synapses. These signals include both local responses to a synapse's milieu and nuclear alterations in gene transcription, and neurons therefore require that the nucleus receive and interpret signals from the cells periphery (Goodman and Shatz, 1993; Greer and Greenberg, 2008).

One potential nexus for the interaction of local and nuclear signaling is the importin protein family. These proteins have a canonical function as nuclear import receptors that regulate transport from the cytoplasm to the nucleus, thereby fulfilling the need of proteins larger than 30–60 kDa to transit the nuclear pore in an actively catalyzed manner (Paine et al., 1975; Peters, 1983; Görlich and Kutay, 1999). Because nuclear entry can be a carefully regulated process for many signaling molecules that govern transcription, importins are critical to regulating neuronal properties (Otis et al., 2006; Ting et al., 2007; Perry and Fainzilber, 2009).

There are over 20 importin genes in mammals. This diversity permits the specialization of importins for particular cargo classes and the independent and tissue-specific regulation of their nuclear import (Fried and Kutay, 2003). In the classical nuclear import pathway, a cargo containing a nuclear localization signal binds to an importin-α, which in turn binds to an importin-β. The latter, via its interactions with nucleoporins, shuttles the heteromer–cargo complex into the nucleus (Görlich et al., 1995; Moroianu et al., 1995). Importin-βs however, can also promote nuclear entry by direct interaction with cargo independent of an

Received July 31, 2009; revised Feb. 11, 2010; accepted March 1, 2010.

This work was supported by National Institutes of Health (NIH) Grants RO1 NS041062 and MH075058 (T.L.S.) and EY03592 (I.A.M.), and predoctoral fellowships from NIH/National Institute of Neurological Disorders and Stroke Ruth L. Kirschstein National Research Service Award (M.E.H.K.), the National Defense Science and Engineering Graduate Fellowship (T.J.M.), and the Howard Hughes Medical Institute (D.K.D.). We thank D. Schmucker for assistance in generating transgenic flies, D. Allan for intellectual input and *Drosophila* stocks, T. Herman for R7 photoreceptor projection analysis, A. Deb and E. Pogoda for technical assistance, and L. Bu of the Mental Retardation Developmental Disabilities Research Center Imaging Core under the support of National Institute of Child Health and Human Development Grant P30HD18655 for imaging assistance. We thank A. DiAntonio, N. Reist, P. ten Dijke, M. Noll, W. Boll, and M. Gonzales-Gaitan for antibodies and *Drosophila* stocks. We also thank the Bloomington Stock Center at the University of Indiana for fly stocks and the Developmental Studies Hybridoma Bank at the University of Iowa for antibodies.

Correspondence should be addressed to Thomas L. Schwarz, F. M. Kirby Center for Neurobiology, Children's Hospital, 300 Longwood Avenue, CLS 12120, Boston, MA 02115. E-mail: thomas.schwarz@childrens.harvard.edu.

D. K. Dickman's present address: Department of Biochemistry and Biophysics, University of California, San Francisco, 1550 Fourth Street, San Francisco, CA 94158.

DOI:10.1523/JNEUROSCI.3739-09.2010

 0270-6474/10/305253-16$15.00/0

importin-α (Görlich and Kutay, 1999). Directionality is tightly regulated by the small GTPase Ran, which is GTP-bound in the nucleus, where it dissociates importins from their cargo (Rexach and Blobel, 1995; Görlich and Kutay, 1999).

Importins, however, are not spatially restricted to the nucleus and can occupy roles beyond that of nuclear gatekeeper (Jakel et al., 2002; Vrailas et al., 2006; James et al., 2007). In the nervous system, particularly, they have gained significant attention for their role in synapse targeting (Ting et al., 2007) and signaling from the periphery to the nucleus (Otis et al., 2006; Perry and Fainzilber, 2009). Axonal injury causes the local translation of importin-β, which then translocates with its cargo to the soma to promote neurite re-outgrowth (Hanz et al., 2003; Perlson et al., 2005). Similarly, synaptic stimuli cause importins to move from dendrites to nuclei to effect forms of synaptic plasticity (Thompson et al., 2004; Lai et al., 2008). Importins are thus emerging as fundamental regulators of neuronal function (Otis et al., 2006; Perry and Fainzilber, 2009).

In a forward genetic screen for defective synaptic transmission, mutants were isolated in *Drosophila importin-β11* (*impβ11*), also called *ran-binding protein 11*, one of 12 importins identified in the *Drosophila* genome. In mammalian cells, importin-β11 is required for nuclear import of the ubiquitin conjugating enzyme UbcM2 (Plafker and Macara, 2000; Plafker et al., 2004) and the ribosomal protein rpL12 (Plafker and Macara, 2002), but no neuronal functions are known. Because only one importin-β has been characterized at the *Drosophila* larval neuromuscular junction (NMJ), *importin-β13* (Giagtzoglou et al., 2009), we undertook to characterize the *impβ11* mutants. We found that loss of *impβ11* caused a local misregulation of bone morphogenic protein (BMP) signaling at the larval NMJ, which resulted in a reduction in both the number of boutons and synaptic transmission.

Materials and Methods

Fly stocks. *Impβ11* alleles were isolated as described previously (Dickman et al., 2005). The *y,w;FRT42D GMR-hid y+ cl 2R/CyO;EGUF/EGUF* parental stock used in the mutagenesis was described previously (Stowers and Schwarz, 1999).

Five independent alleles of *impβ11* were isolated and mapped using the deficiencies *Df(2R)ΔM22-103* (*Poxn*$^{\Delta M22\text{-}103}$), a generous gift from M. Noll and W. Boll (University of Zurich, Zurich, Switzerland) (Boll and Noll, 2002), *Df(2R)Jp1*, and *Df(2R)Jp5* (Bloomington Stock Center) followed by genomic sequencing to identify the precise molecular lesions. For all experiments, the control genotype was *y,w; FRT42D* (Xu and Rubin, 1993), whereas for *impβ11* mutants, the *impβ11*^{70} allele was used in trans to the genomic deficiency *Df(2R)ΔM22-103*.

UAS-impβ11-eGFP was generated by cloning the full-length cDNA (EST, LD41918; Invitrogen) into the *pUAST* vector (Brand and Perrimon, 1993) using PCR-added *Bgl*II and *Kpn*I sites. Enhanced green fluorescent protein (eGFP) was ligated in frame into the *pUAST-impβ11* construct using engineered *Kpn*I and *Xba*I sites. Transgenic flies were generated by standard transformation methods (Rubin and Spradling, 1982).

All fly stocks were raised in humidified incubators at 25°C. Third-instar larvae were grown in low-density cages at 25°C on agar grape plates with yeast paste.

The following stocks were also used: *elav-Gal4* (Luo et al., 1994); *da-Gal4* (Wodarz et al., 1995); *G14-Gal4*, *OK6-Gal4*, *wit*^{A12}, *wit*^{B11}, *wit*^{HA1} (Aberle et al., 2002); *n-syb*$^{F\text{-}33R}$ (Deitcher et al., 1998); *MAD*^{10} (Sekelsky et al., 1995); *UAS-gbb*$^{9.1}$ (S. Thor, Linköping University, Linköping, Sweden); (Wharton et al., 1999); *UAS-tkv*^{Q253D} (mobilized onto X by D. Allan, University of British Columbia, Vancouver, BC Canada) (Nellen et al., 1996); *UAS-sax*^{Q263D} (mobilized onto X by D. Allan) (Haerry et al., 1998); *UAS-GFP-MAD* (Dudu et al., 2006); *UAS-dynamitin* (D. Allan) (Duncan and Warrior, 2002); *tubulin-GAL4* (Lee and Luo, 1999); *UAS-wit* (Marqués et al., 2002). Stocks were obtained from the Bloomington Stock Center when available.

Antibody production. A PCR fragment with flanking 5′ *Eco*RI and 3′ *Ava*I sites encoding importin-β11 amino acids 923 to 1075 was amplified and cloned into the pGEX-4T-1 vector (GE Healthcare) using the following primers: 5′ GST-RanB2- GAA TTC GGC GAA GTG ATG GAC AA 3′ GST-RanB2-GAG CTC CGG CCT GAG GTG GAC AA. The fidelity of the clone was verified by sequencing throughout the entire open reading frame. Subsequently, the 51 kDa glutathione *S*-transferase (GST) fusion protein was expressed in and purified from *Escherichia coli* BL21 cells using the Bulk GST Fusion Purification Module according to the manufacturer's protocols (GE Healthcare). The resultant protein was injected into naive New Zealand white rabbits (Covance). Crude antisera were then affinity purified over an Affi-Prep 10 column (Bio-Rad) containing the original fusion protein to which the antibody was raised. Affinity-purified antibody was eluted from the column by standard methods (Harlow and Lane, 1988) in 100 mM glycine, pH 2.3, and neutralized in 1 M Tris base, pH 7.5. The antibodies were then dialyzed with PBS containing 5% BSA. Antibodies were tested by recognition of a 110 kDa band by Western blot corresponding to the predicted molecular weight of importin-β11 that was absent in null mutants. One antibody, 5157, was found to recognize endogenous and exogenous importin-β11 and was used for subsequent studies.

Germline clones. The following stocks and genotypes were used: (1) *y,w, hs-FLP; FRT42D imp-β11*^{70}*/CyO*; (2) *y,w, hs-FLP; FRT42D*; (3) *y,w; FRT42D imp-β11*^{70}*/Cyo, GFP [CyO, P(ActGFP)]*; (4) *y,w; FRT42D*; (5) *w[*]; P{w[+mW.hs]=FRT(w[hs])}G13 P{w[+mC]=ovoD1-18}2R/Dp(?;2)bw[D], S[1] wg[Sp-1] Ms(2)M[1] bw[D]/CyO; +; + (BL 2125)*; (6) *y,w, hs-FLP/y,w; FRT42B ovo*^{D}*/FRT42D imp-β11*^{70}; (7) *y,w, hs-FLP/y,w; FRT42B ovo*^{D}*/FRT42D*.

Germline clones were generated using the dominant female sterile technique using the *ovo*^{D} mutation and a source of FLPase under the control of a heat-shock promoter (Chou and Perrimon, 1992, 1996). In experimental conditions, *FRT42B ovo*^{D}-bearing males were crossed to *y,w, hs-FLP; FRT42D impβ11*^{70}*/CyO* virgins. The progeny were heat shocked at 37°C starting in the second instar for 1 h per day for 6 consecutive days to induce recombination. Though the recombination of 42B and 42D is expected to cause a chromosomal deletion between these two loci, this deletion has been shown previously to have no impact on the production of viable embryos (Murthy et al., 2005). Indeed, control crosses using the parental 42D chromosome resulted in embryos that developed into normal adults. Resultant virgin female adults of the genotype *y,w, hs-FLP/y,w; FRT42B, ovo*^{D}*/FRT42D, impβ11*^{70} were then mated to *y,w; FRT42D, impβ11* ^{70}*/Cyo, GFP [CyO, P{ActGFP}]* with the intent to select against GFP-bearing balancer chromosomes to ensure both a germline null and a zygotic null. Results were confirmed independently using the *impβ11* ^{20} allele.

Immunostaining. Third-instar larval fillets were fixed in 4% paraformaldehyde for 20 min. Antibody staining was performed in PBS containing 0.3% Triton X-100 and 5% normal donkey serum. Fillets were mounted in Vectashield (Vector Labs). Adult recombinant heads were prepared as described previously (Stowers et al., 2002) with the exception of fixation conditions (3.7% formaldehyde in 100 mM potassium phosphate, pH 6.8, 450 mM KCl, 150 mM NaCl, and 20 mM $MgCl^2$) and sectioned using a Leica CM3050S cryostat. For comparisons, animals were stained concurrently, imaged, and processed identically.

The following antibodies were used: anti-Chaoptin 24B10 [1:100; Developmental Studies Hybridoma Bank (DSHB)]; rabbit anti-synaptotagmin I (Syt I; 1:4000) (Mackler et al., 2002); mouse anti-Bruchpilot (BRP), nc82 (1:100) (Hofbauer et al., 2009); mouse anti-GluRIIA (1:100; DSHB); rabbit anti-GluRIIB, (1:2500) (Marrus et al., 2004); rabbit anti-GluRIIC (1:2000) (Marrus and DiAntonio, 2004); rabbit anti-phosphorylated mothers against decapentaplegic (pMAD), PS1 (1:2000) (Persson et al., 1998); mouse anti-Fasciclin II (FasII), 1D4 (1:20; DSHB); mouse anti-Futsch, 22C10 (1:100; DSHB); rabbit anti-Thickveins (Tkv) (1:1250) (McCabe et al., 2004); mouse anti-Wishful thinking (Wit), 23C7 (1:10) (Aberle et al., 2002; Wang et al., 2007); goat anti-MAD (1:100; Santa Cruz Biotechnology) (Zhu et al., 1999; Li and Li, 2006); cyanine 5

(Cy5)- or FITC-conjugated goat anti-HRP (1:100; Jackson ImmunoResearch); Alexa Fluor 594-conjugated wheat germ agglutinin at 5 μM (Invitrogen); FITC- or Cy3-conjugated secondary antibodies (1:200; Jackson ImmunoResearch).

Imaging and analysis parameters. All images were processed using a Zeiss LSM 510 Meta laser scanning confocal microscope and either a 63×, 1.4 numerical aperture (NA) or 40×, 1.0 NA oil-immersion objective. Laser scanning microscope software and Adobe Photoshop (Adobe Systems) were used for image processing. For bouton quantification, larvae were stained with antibodies to HRP and boutons counted on muscles 6 and 7 in segment A2. Muscle surface area was calculated from 10× differential interference contrast micrographs of muscle fields; the length and width of each muscle were used to calculate a surface area. Statistics were performed as repeated-measurement ANOVA tests with a *post hoc* Dunnett's multiple comparison test between all combinations of genotypes. BRP, GluRIIA, GluRIIB, and GluRIIC puncta were manually counted at MN4b synapses on muscle 4. Terminal area was calculated using the threshold function in MetaMorph for the HRP channel. Statistical analysis was conducted using GraphPad Prism 5 software and significance values were calculated using an unpaired Student's *t* test. All histograms and measurements are shown as mean ± SEM; sample size (*n*) is described either in the figure legends or in the Results section.

Electrophysiology. NMJ recordings were performed as described previously (Dickman et al., 2005). Briefly, recordings were conducted in HL3 saline solution (Stewart et al., 1994) containing 20 mM Mg^{2+} and either 1 mM Ca^{2+} or 0.6 mM Ca^{2+} as indicated. All physiology was recorded from muscle 6 in abdominal segments A2 to A4. Recordings conducted on muscles with membrane potentials (V_m) of −55 mV or less were included for analysis. Quantal content was corrected for nonlinear summation (Martin, 1955).

Electroretinograms (ERGs) were performed as described previously (Dickman et al., 2005). HL3 saline solution was used in the stimulating electrode placed in the thorax of the adult fly. The recording electrode was filled with 3 M KCl and placed on the surface on the eye. Light stimuli lasted 1 s.

Philanthotoxin (PhTx) homeostasis experiments were conducted as described previously (Goold and Davis, 2007). A final concentration of 4 μM PhTx in 1 mM Ca^{2+} HL3 saline was applied to a semi-intact larval preparation for 10 min. The PhTx was washed out, and recordings were made as above.

Statistics were calculated using ANOVA followed by a Bonferroni post-comparison test (GraphPad). All histograms and measurements are shown as mean ± SEM; sample size (*n*) is described either in the figure legends or in the Results section.

Electron microscopy. Laminas innervated by either control or *impβ11* mutant photoreceptors were prepared for electron microscopy (EM) using previously reported methods (Meinertzhagen, 1996). Single sections containing cartridge profiles cut in fair cross-section were examined, and digital montages were collected from images obtained with a Philips Tecnai 12 electron microscope operated at 80 kV, using a Kodak Megaview II camera with software (AnalySIS; Soft Imaging System).

We made counts of the following organelle profiles: ~30 nm synaptic vesicles, T-bar presynaptic ribbons at tetrad synapses, and glial invaginations into R1–R6 terminals, called capitate projections. The perimeters and cross-sectional areas of terminal profiles were measured with software (NIH ImageJ) to determine the packing density of synaptic vesicle profiles. Tests for statistical significance in organelle counts were first made by an unweighted means ANOVA, followed by Tukey's honestly significant difference test using software (Systat version 5.2.1). Error bars in figures indicate mean ± SEM.

Immunoblots and SDS-PAGE analysis. For immunoblots, extracts were made from timed embryo collections or from intact third-instar larvae by drop-freezing specimens in liquid N_2 and homogenizing them directly in 2× Laemmli buffer (Laemmli, 1970). Synaptosome fractions were prepared from adult heads as described previously (Kelly, 1983) in synaptosome buffer (10 mM HEPES, pH 7.5, 1 mM $MgCl_2$, 0.32 M sucrose). Proteins were separated on 8% polyacrylamide gels and transferred to nitrocellulose membranes. Primary antibodies were applied overnight at 4°C, and secondary antibodies for 1 h at 21°C. The following antibodies were used: rabbit anti-importin-β11 (1:7500; present study); mouse anti-Bruchpilot (1:100) (Hofbauer et al., 2009); mouse anti-Lamin C LC28.26 and anti-Lamin D_m0 ADL101 (1:5000) (Riemer et al., 1995); and mouse anti-α-tubulin (1:25,000; Sigma-Aldrich). HRP-conjugated secondary antibodies (Jackson ImmunoResearch) were used at 1:10,000 (anti-mouse) or 1:20,000 (anti-rabbit). Blots were developed using the SuperSignal West Dura Extended Duration Substrate Kit (Thermo Scientific).

Fluorescence intensity measurement. Fluorescence from the neuronal marker anti-HRP was used to generate a region of interest (ROI) around the synaptic terminal using the thresholding function. Integrated fluorescent intensity was then measured within the ROI in arbitrary units and divided by the area of the ROI. MetaMorph software (Molecular Devices) was used for all measurements and analyzed using ANOVA followed by a Bonferroni post-comparison test or Student's *t* test analysis (GraphPad Prism). All histograms and measurements are shown as mean ± SEM.

Results

Photoreceptor neurotransmission defects in *impβ11* mutants

A lethal complementation group consisting of five *impβ11* mutant alleles (70, 9, 24, 20, and 202) was isolated in a forward genetic screen that has previously yielded a collection of mutants with defective synaptic development and transmission (Stowers et al., 2002; Dickman et al., 2005, 2008; Pack-Chung et al., 2007). This screen examined flies whose eyes were completely homozygous for a mutated chromosome arm 2R while the rest of the fly was heterozygous for that chromosome (Stowers and Schwarz, 1999). A primary screen selected flies that failed to perform phototaxis, and was followed by a secondary screen for abnormalities in the ERG. Each allele of the complementation group described here failed to complement the x-ray-induced deficiency *Df(2R)ΔM22-103* (hereafter referred to as *Df*; a generous gift from W. Boll and M. Noll). With partially overlapping deficiencies (Fig. 1*A*), the location of the alleles was restricted to an area bordered by the genes *vha36* and *poxn* in the cytological region 52C. Sequencing of candidate genes revealed nonsense mutations in all five alleles in *impβ11*, whose closest homologs include human importin-β11 and yeast Kap120p/Lph2p sharing 34% and 23% amino acid identity, respectively (Plafker and Macara, 2000; Caesar et al., 2006). The sequence of *impβ11* predicts a protein of 1075 aa. At the N terminus, it possesses a conserved Ran-binding domain characteristic of all importin-βs (Fig. 1*B*, RBD). This region is followed by a long C-terminal region that shares homology only with the β11 class of importins. Three alleles introduced a stop codon before or just at the beginning of the Ran-binding domain (Fig. 1*B*). Given that the Ran-binding domain is essential for nuclear import and most of the protein is absent, these are likely null alleles. The remaining two alleles, although independently derived, introduced stop codons at the same position, amino acid 853 (Fig. 1*B*). All alleles, when placed over the deficiency (*Df*), failed to produce a full-length protein (Fig. 1*E*).

When these alleles were made homozygous selectively in the eye (Stowers and Schwarz, 1999), their ERGs lacked "on" and "off" transients in response to brief exposures to light (Fig. 1*C*, arrows). These transients are reported to arise from the synchronous activation of second-order cells in the visual system (Coombe, 1986); their absence indicates a failure of normal transmission by the photoreceptors. In contrast, the persistence of the sustained negative phase of the response indicates that the phototransduction cascade remained intact (Heisenberg, 1971). The four additional alleles displayed a similar ERG profile (data not shown; $n \geq 4$). Thus, the *impβ11* mutants were defective at a step downstream of the depolarization of the photoreceptor but

upstream of activating the target neurons. We were able to fully restore the on and off transients by specifically expressing a *UAS-impβ11-eGFP* transgene in the photoreceptors by means of *ey-GAL4* (Fig. 1*C*) (Brand and Perrimon, 1993; Hazelett et al., 1998; Stowers and Schwarz, 1999). The successful rescue indicates that the ERG defect resulted from loss of importin-β11 and not from potential second-site mutations.

The ERG defect could have arisen from a functional defect in transmission or a developmental defect in the connections made by the photoreceptors. To analyze the photoreceptor axon projections, adult heads with homozygous mutant eyes were sectioned at 10 μm with a cryostat, and photoreceptors were immunolabeled with a photoreceptor-specific antibody against Chaoptin. No gross abnormalities were detected in these projections: R1–R6 endings appeared to terminate appropriately in the lamina, and normal terminals appeared in the layers of the medulla that receive the endings of photoreceptors R7 and R8 (Fig. 1*D*). In electron micrographs of the lamina from animals with homozygous mutant photoreceptors (*y,w;FRT42D, impβ11^{70}/FRT42D, GMR-hid, cl;EGUF/+*), the ordered structure of the cartridges containing endings of the R1–R6 photoreceptors appeared normal, and synapses were identified with appropriate T-bar ribbons, presynaptic densities, and clusters of vesicles. Small clear vesicles were normal in size but more numerous at mutant terminals (supplemental Fig. S1*A*,*B*, available at www.jneurosci.org as supplemental material), a phenotype consistent with a decrease in vesicle release (Hiesinger et al., 2006). The cross-sectional area of the terminal profile was also significantly increased resulting in normal vesicle density (supplemental Fig. S1*C*,*D*, available at www.jneurosci.org as supplemental material). In addition, capitate projections were almost absent from mutant terminals, a phenotype that has been interpreted previously to result from decreased endocytosis, a likely consequence of decreased vesicle release (supplemental Fig. S1*E*, available at www.jneurosci.org as supplemental material) (Fabian-Fine et al., 2003).

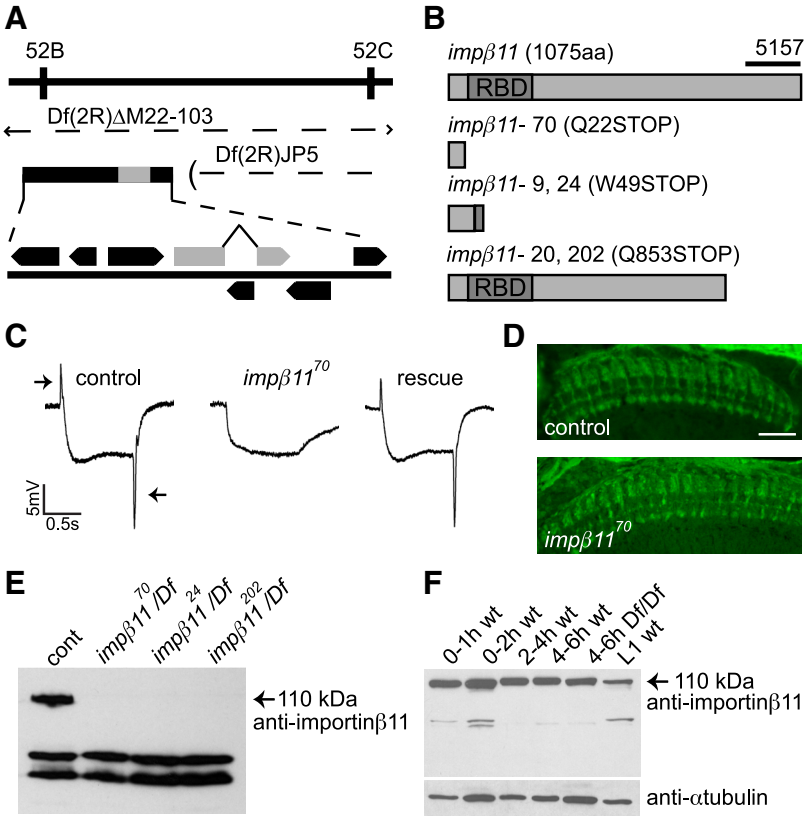

Figure 1. *impβ11* mutants have defective photoreceptor neurotransmission but normal projections. ***A***, The genomic region of a complementation group isolated in the EGUF-hid screen was narrowed using two overlapping deficiencies, *Df(2R)ΔM22-103* and *Df(2R)JP5*, which contain the indicated predicted open reading frames, including the gene *ran-binding protein 11* or *importin-β11* (gray). ***B***, Schematic of wild-type importin-β11 with the Ran-binding domain (RBD) marked, and the predicted products of each allele. Although independently derived, identical point mutations were shared by alleles 9 and 24 and alleles 20 and 202. The antibody 5157 was raised against the C-terminal region (bar). ***C***, Representative responses to light (between arrows) from control (*y,w; FRT42D, GMR-hid 2R, CL/CyO; EGUF*), *impβ11^{70}* mutant eyes (*y,w; FRT42D, GMR-hid 2R, CL/FRT42D, impβ11^{70}; EGUF*), and *impβ11^{70}* mutant eyes expressing a *UAS-impβ11-eGFP* transgene (*y,w; FRT42D, GMR-hid 2R, CL/FRT42D, impβ11^{70}; EGUF/UAS-impβ11-eGFP*). On and off transients (arrows) were absent from *impβ11^{70}* eyes but rescued by the transgene ($n \geq 7$ for each genotype). ***D***, Representative confocal images of photoreceptors stained with anti-Chaoptin. Homozygous *impβ11^{70}* R7 and R8 cells terminate in appropriate layers in the medulla ($n \geq 4$ for each genotype). Scale bar, 20 μm. ***E***, In lysates of third-instar larvae, the antibody generated against importin-β11 recognizes a band at the predicted molecular weight of 110 kDa that is absent in all *impβ11* mutant alleles. Nonspecific bands of lower molecular weight persisted in the null larvae. ***F***, Reflecting the presence of maternally contributed protein or mRNA, importin-β11 was detected at all embryonic stages in both control (wt) animals and *Df(2R)ΔM22-103* homozygous nulls (*Df/Df*).

Importin-β11 expression in the larval nervous system

Each *impβ11* allele, when placed over the *Df*, was lethal at the pharate adult stage, indicating that its function was not restricted to photoreceptors. To determine the developmental profile of importin-β11, we generated an antiserum (5157) to amino acids 923 to 1075 (Fig. 1*B*). On immunoblots of homogenates of third-instar larvae, this antiserum detected a band of the predicted molecular weight, 110 kDa, that was absent from *impβ11^{70}/Df* (Fig. 1*E*). Nonspecific bands of 70 and 60 kDa were also observed that could not be removed by affinity purification.

Importin-β11 protein was detected throughout the life cycle in wild-type animals, including lysates from embryos aged 0 to 2 h after egg deposition, a stage before initiation of zygotic transcription (Fig. 1*F*) (Anderson and Lengyel, 1979). In addition, lysates of homozygous *Df* embryos had a detectable band at 110 kDa (Fig. 1*F*). Because this deficiency removes the entire *impβ11* gene, this early expression must result from maternally contributed mRNA or protein. We reasoned that maternally derived importin-β11 might mask the requirements for this protein before the pupal stage. Therefore, we used the ovo^{D} method (Chou and Perrimon, 1992, 1996) to generate maternal germline clones homozygous for the *impβ11^{70}* and *impβ11^{20}* alleles. Mutant females did not lay eggs, and on examination of mutant ovarioles, the ovo^{D} phenotype was evident, consistent with the hypothesis that importin-β11 plays an essential role in the female germline (Chan et al., 2008). Hereafter, unless otherwise notated, late third-instar larvae of genotype *y,w;FRT42D, impβ11^{70}/Df* were used for experiments and will be referred to as *impβ11* null lar-

vae. At this stage, maternally supplied importin-β11 was no longer detectable by Western blot in this genotype (Fig. 1*E*).

Third-instar larvae offered us the advantage of using homozygous mutant animals to characterize the phenotype at the NMJ, a synapse amenable to both anatomical and electrophysiological analysis (Schwarz, 2006). Identifiable motor neurons exit the larval ventral nerve cord (VNC) and innervate specific muscles in each hemisegment of the body wall, where they form synaptic varicosities or boutons (Keshishian et al., 1996).

To examine importin-β11 immunoreactivity at these NMJs, body wall preparations were labeled with antiserum 5157 (Fig. 2*A–F*). In control body walls, muscle nuclei were immunoreactive, and the protein was enriched in puncta on the nuclear envelope, presumably corresponding to nuclear pores (Fig. 2*B*). This immunoreactivity was absent in *impβ11* mutants (Fig. 2*C*,*D*). The antibody also labeled the NMJ (Fig. 2*A*,*E*), but this signal was not caused exclusively by importin-β11 because it was also present at mutant NMJs (Fig. 2*C*,*F*). To circumvent this problem, we created a transgenic line (*UAS-impβ11–eGFP*) expressing importin-β11 fused to eGFP and placed under the control of a *UAS* promoter (Brand and Perrimon, 1993). When expressed either ubiquitously (with a *da-GAL4* driver) (Wodarz et al., 1995) or exclusively in the nervous system (with an *elav-GAL4* driver) (Luo et al., 1994), but not when expressed in muscle (with a *G14-GAL4* driver) (Aberle et al., 2002), this construct rescued the lethality of *impβ11* null larvae, indicating both that the transgene was functional and that lethality at the pupal stage was attributable to an essential neuronal function of importin-β11.

In the nervous system, importin-β11-eGFP protein localized to puncta in axons, to the cytoplasm and nuclei of many cells in the VNC, including motor neurons, and in the neuropil, the synaptic region of the VNC (Fig. 2*G–I*). As expected for a nuclear import factor, at high magnification, importin-β11-eGFP was observed at the nuclear envelope of these neurons where it concentrated at nuclear pores (Fig. 2*J*). Consistent with the importin-eGFP signal in nerves and the synaptic neuropil, neuronally expressed importin-β11-eGFP was also present at presynaptic neuromuscular terminals (Fig. 2*K*,*L*). The fluorescent importin-β11, however, was only prominent in ~30% of body wall NMJs in any given larva, and filled some but not all boutons within a given synapse (Fig. 2*L*). This irregular distribution likely reflects the pattern of expression of the GAL4 line *elav-GAL4*, the insertion site of the *UAS-impβ11–eGFP* transgene, or a combination of both. A stronger, ubiquitous driver (*tubulin-GAL4*) (Lee and Luo, 1999) caused importin-eGFP to be visible in all boutons within a given NMJ (Fig. 2*M*). Furthermore, because the NMJ at muscles 6/7 contains the terminals of two axons, we also examined the simpler, singly innervated muscle 4 (Fig. 2*N*) (Lnenicka and Keshishian, 2000; Hoang and Chiba, 2001). Here too, all boutons were positive for eGFP. These data suggest that importin-β11 can localize to synaptic terminals in addition to the synapse-rich region of the VNC, nuclear pores, cell bodies, and muscle nuclei. We also observed importin-β11-eGFP localization to muscle nuclei and trachea when expressed ubiquitously (Fig. 2*M*,*N*). To address whether endogenous importin-β11 could also localize to synapses, we performed a subcellular fractionation of adult head lysates (Kelly, 1983). As expected, importin-β11 immunoreactivity was detected in the nuclear fraction, on long exposure, but it also appeared in the synaptosome fraction and in the cytosol (supplemental Fig. S2, available at www.jneurosci.org as supplemental material). Thus, importin-β11 is likely to mediate import through nuclear pores in both neurons and muscle cells, but may also have a function at synaptic terminals.

Structural and functional defects at the *impβ11* mutant NMJ

Because we could detect a synaptic pool of importin-β11, we next examined the NMJ for potential structural and developmental phenotypes by counting the number of boutons present at the NMJ in wild-type and *impβ11* mutant larvae. Although the size of their muscle fibers was normal, *impβ11* mutant larvae had a 30% reduction in bouton number when compared to either control larvae or heterozygote mutant larvae (Fig. 3*A*,*B*). Bouton counts are frequently expressed normalized to muscle surface because bouton number is known to scale with muscle size during development (Lnenicka and Keshishian, 2000; Marqués et al., 2002). Thus, normalized to account for variations in larval size, *impβ11* null mutants showed a similar 30% decrease in bouton density (Fig. 3*B*). Synaptic footprints, a sign that boutons have retracted (Eaton et al., 2002), were scant in both mutant and control (control, zero footprints in ~300 boutons; *impβ11*, two footprints in ~500 boutons). Therefore, the altered bouton number likely reflects a reduction in bouton addition as the terminal developed.

Inputs from both type Ib (large) and type Is (small) boutons contribute to the synaptic arbor and electrophysiological profile (Johansen et al., 1989; Lnenicka and Keshishian, 2000). There was no preferential loss of Ib or Is boutons in *impβ11* NMJs, but arbor length and bouton diameter were both slightly decreased when compared to control (data not shown). In addition, the geometry of the synapse was altered in *impβ11* mutants with axonal branches remaining close to the intermuscular cleft rather than spreading across the width of the muscle (Fig. 3*A*).

To determine whether the reduction in bouton number was primarily the result of presynaptic or postsynaptic defects, we expressed *UAS-impβ11-eGFP* in all tissues (with a *da-GAL4* driver), in neurons (with an *elav-GAL4* driver), or in muscle (with a *G14-GAL4* driver). The reduction in bouton number/muscle surface area was statistically rescued to control values when *impβ11-eGFP* was expressed in all cells and in neurons alone, but not by expression in muscle alone (Fig. 3*B*) (control, $0.88 \pm 0.048/1000\ \mu m^2$; $imp\beta11^{70}/Df$, $0.62 \pm 0.044/1000\ \mu m^2$; all cells rescue, $0.93 \pm 0.036/1000\ \mu m^2$; neuron rescue, $0.92 \pm 0.034/1000\ \mu m^2$; muscle rescue, $0.61 \pm 0.029/1000\ \mu m^2$; $n \geq 17$ for each genotype). Thus, importin-β11 is primarily required presynaptically for normal bouton formation and arborization.

To determine whether these structural defects were accompanied by electrophysiological defects, we stimulated the motor nerve that innervates muscle 6 to evoke excitatory junctional potentials (EJPs). Consistent with the morphological defects, the amplitude of EJPs was reduced by 40% in the mutant larvae as compared with control (Fig. 3*C*,*E*) (control, 35.6 ± 1.08 mV; *impβ11*, 21.1 ± 1.81 mV; $n \geq 12$ for both genotypes). Vesicles also fuse spontaneously at the NMJ, giving rise to quantal events or miniature EJPs (mEJPs). mEJPs were also altered (Fig. 3*D*,*F*,*G*); *impβ11* released vesicles at a lower frequency, about 65% less than control (Fig. 3*F*) (control, 3.34 ± 0.367 Hz; *impβ11*, 1.19 ± 0.171 Hz; $n \geq 11$ for both genotypes). This decrease could, at least in part, reflect fewer release sites in the smaller synaptic arbor. There was also a small, but statistically significant, decrease in the amplitude of the mEJPs (Fig. 3*G*) (control, 0.95 ± 0.052 mV; *impβ11*, 0.77 ± 0.035 mV; $n \geq 11$ for both genotypes), suggesting that *impβ11* mutants may have a mild reduction in postsynaptic receptor density or sensitivity (Petersen et al., 1997; DiAntonio et al., 1999). As calculated from these data, quantal content, or the number of vesicles released per

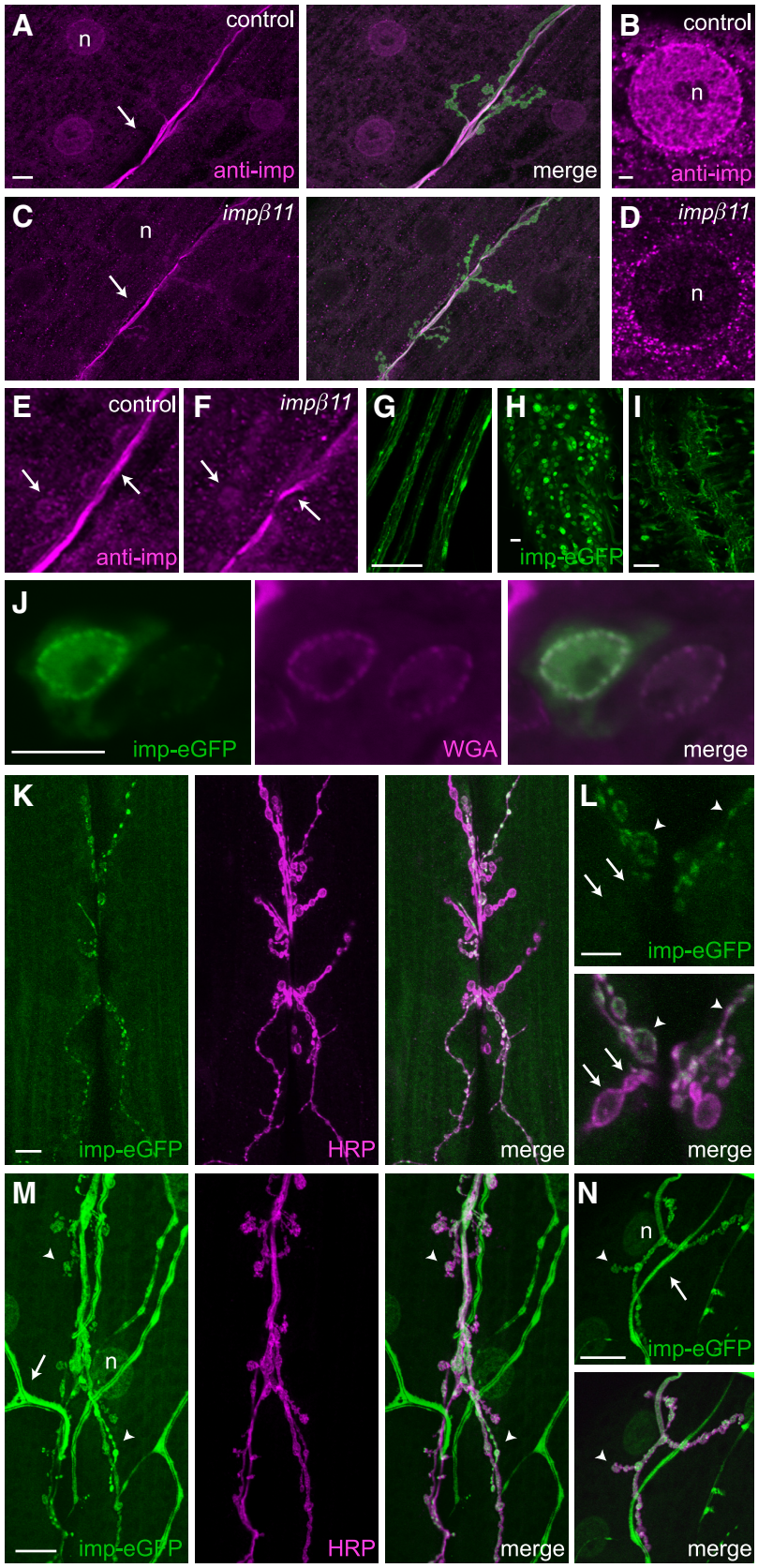

Figure 2. Importin-β11 localization in third-instar larvae. ***A–F***, Representative confocal images of NMJs and muscle fields immunostained with the rabbit antiserum 5157 against importin-β11 (magenta) and the neuronal membrane marker anti-HRP (green). ***A***, ***B***, Immunoreactivity was present in control muscle nuclei (n) and enriched around the nuclear envelope, but was not in *impβ11* muscles (***C***, ***D***). ***A***, ***C***, ***E***, ***F***, At the NMJ, immunoreactivity unrelated to importin-β11 was detected both in control and *impβ11* NMJs (arrows). ***G–J***, *UAS-impβ11-eGFP* expressed in the nervous system with *elav-GAL4*, localized to puncta in the segmental nerves (***G***), and in the VNC to neuronal cell bodies and nuclei (***H***), neuropil (***I***), and nuclear pores (***J***). Nuclear pores were identified with fluorescently conjugated wheat germ agglutinin (magenta) (Finlay et al., 1987). ***K***, ***L***, When driven with *elav-GAL4*, *impβ11-eGFP* was present in most type Ib and Is boutons (arrowheads) of the anti-HRP-stained NMJ, but was not detected in some (arrows). ***M***, ***N***, When importin-eGFP was driven with a stronger driver, *tubulin-GAL4*, eGFP signal was visible in all boutons at muscles 6/7 (***M***, arrowheads) and 4 (***N***, arrowheads). eGFP signal was also detected in muscle nuclei (n) and trachea (arrows). Scale bars: ***A*** (for ***A***, ***C***), ***G–I***, ***K***, ***M***, ***N***, 20 μm; ***B*** (for ***B***, ***D***), ***J***, ***L***, 5 μm. Genotypes are as follows: ***A–F***, *y,w; FRT42D*; ***G–L***, *FRT42D, impβ11^{70}/+; elav-GAL4/UAS-impβ11-eGFP*; ***M***, ***N***, *FRT42D, impβ11^{70}/Df; tubulin-GAL4/UAS-impβ11-eGFP*.

action potential, was reduced by 30% in *impβ11* (Fig. 3*H*) (control, 43.3 ± 2.40; *impβ11*, 30.7 ± 2.82; $n \geq 10$ for both genotypes) when corrected for nonlinear summation (Martin, 1955).

Defects in synaptic transmission can result from either presynaptic or postsynaptic mechanisms. We therefore selectively restored function of importin-β11 using *UAS-impβ11-eGFP* in either neurons or muscle. The observed defects in quantal content and EJP amplitude in *impβ11* were fully rescued with expression of the *UAS-impβ11-eGFP* transgene in the nervous system with *elav-GAL4* [EJP amplitude: neuron rescue, 32.3 ± 1.71 mV; muscle rescue, 27.1 ± 1.11 mV (Fig. 3*E*); quantal content: neuron rescue, 50.1 ± 2.71; muscle rescue, 39.7 ± 1.98 (Fig. 3*H*); $n \geq 10$ for each genotype]. Although quantal content was somewhat increased by transgene expression in muscle, it did not correspond to a statistically significant restoration of EJP amplitude. In contrast, neuronal rescue was significant and complete, indicating that neuronal expression of importin-β11 was both sufficient and necessary to rescue the electrophysiological defect (p values compared to control: neuron rescue, $p \geq 0.05$; muscle rescue, $p < 0.0001$; compared to mutant: neuron rescue, $p < 0.0001$; muscle rescue, $p \geq 0.05$). Separately, neither neuronal nor muscle expression of importin-β11-eGFP was adequate to restore mEJP frequency or amplitude to control levels; however, concurrent expression in both neurons and muscle significantly increased mini frequency (Fig. 3*F*) (neuron rescue, 1.64 ± 0.250 Hz, 0.73 ± 0.033 mV; muscle rescue, 1.55 ± 0.314 Hz, 0.76 ± 0.035 mV; all cells rescue, 3.02 ± 0.546 Hz, 0.64 ± 0.025 mV; $p \geq 0.05$ when *da-GAL4* frequency was compared to control; $n \geq 11$ for each genotype). mEJP amplitude was not rescued, and may be partic-

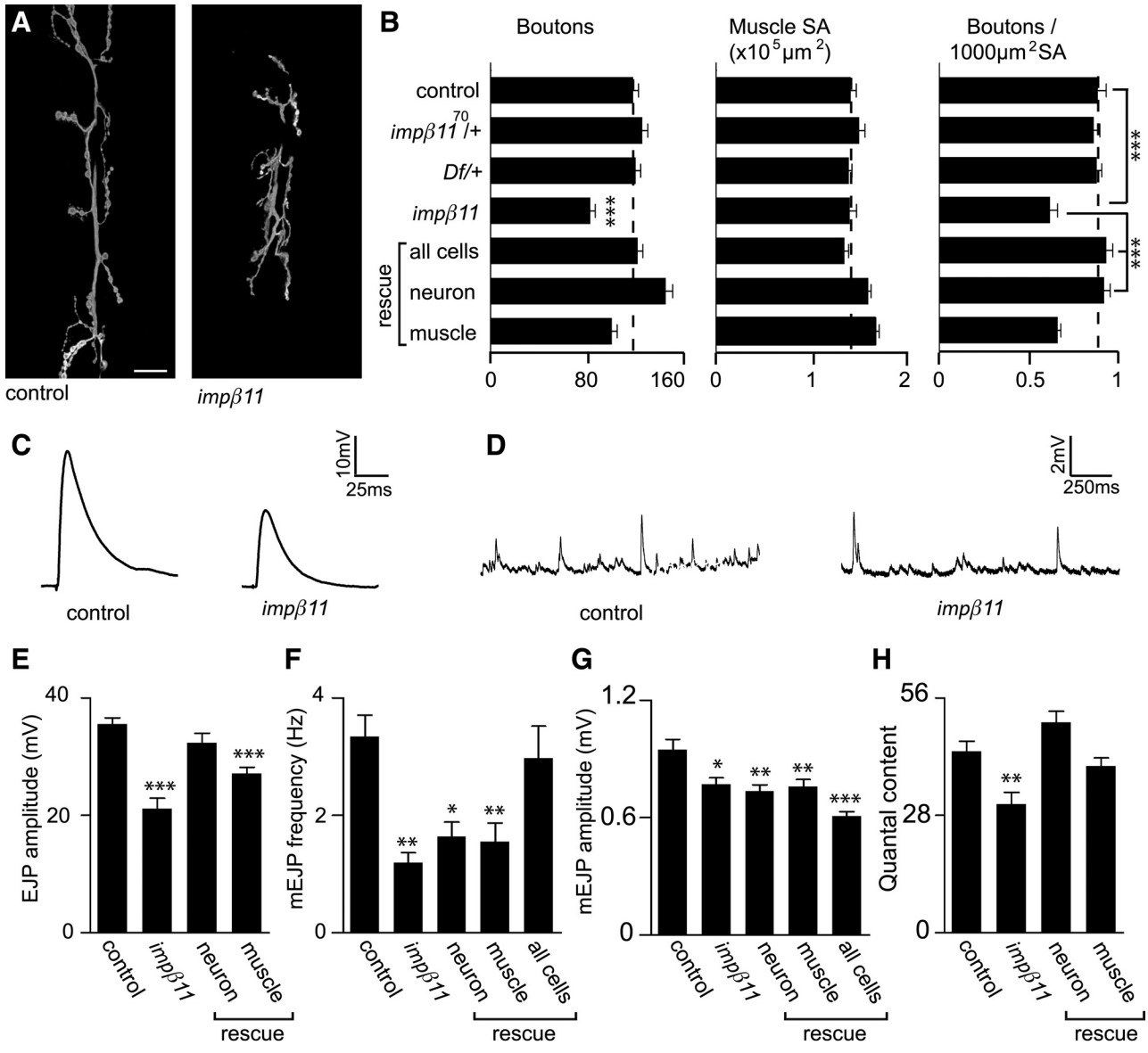

Figure 3. Reduced bouton number and quantal content in *impβ11* mutants. ***A***, Representative confocal images of third-instar larval NMJs stained with anti-HRP. The synaptic arbor in *impβ11* mutant larvae was shorter and narrower. Scale bar, 20 μm. ***B***, Bouton number, muscle surface area, and bouton number normalized to muscle area were calculated for all genotypes. Although muscle size was normal, *impβ11* muscles had fewer boutons than control or heterozygous animals. Bouton number was rescued with *UAS-impβ11-eGFP* transgene expression in all cells (*da-GAL4*) or in neurons (*elav-GAL4*), but not by expression in muscle (*G14-GAL4*). The slight increases in bouton number and muscle size observed with the *G14-GAL4* driver were not seen with *24B-GAL4*, another muscle driver. ***C***, ***D***, Representative EJPs and mEJPs from control and *impβ11* mutant larvae. ***E***, EJP amplitude was reduced in *impβ11* and fully rescued by transgene expression in neurons but not by expression in muscle. ***F***, mEJP frequency was decreased in *impβ11* and was only fully rescued with *impβ11* transgene expression in both presynaptic and postsynaptic compartments with *da-GAL4*. ***G***, mEJP amplitude was slightly reduced in *impβ11*, but was not restored by transgene expression. ***H***, Quantal content, corrected for nonlinear summation, was reduced in *impβ11* and rescued by transgene expression in neurons. Recordings were conducted in 1 mM Ca^{2+} HL3. $^{*}p < 0.05$; $^{**}p < 0.001$; $^{***}p < 0.0001$ compared to control. Genotypes are as follows: control (*y,w; FRT42D*), *impβ11* (*FRT42D, impβ11^{70}/Df*), all cells (*FRT42D, impβ11^{70}/Df; da-GAL4/UAS-impβ11-eGFP*), neuron rescue (*FRT42D, impβ11^{70}/Df; elav-GAL4/UAS-impβ11-eGFP*), muscle rescue (*FRT42D impβ11^{70}, G14-GAL4/Df; UAS-impβ11-eGFP/+*).

ularly sensitive to appropriate expression levels of the importin. Thus, presynaptic importin-β11 was sufficient to restore bouton number and EJP amplitude, suggesting that importin-β11 at the presynapse was required for normal NMJ arborization and function.

To further characterize *impβ11* abnormalities at the NMJ, we examined proteins of known importance to the development and function of this synapse. Several structural components were investigated that could potentially contribute to the phenotype. However, both the cell-adhesion molecule FasII and the microtubule-associated protein Futsch (Schuster et al., 1996; Hummel et al., 2000; Roos et al., 2000) localized normally in *impβ11* mutant NMJs (supplemental Fig. S3, available at www.jneurosci.org as supplemental material). The reduction in bouton number was therefore not likely to arise from gross abnormalities in these structural components. Similarly, Syt I immunolabeling indicated that synaptic vesicles were concentrated within boutons (Fig. 4*A*) (DiAntonio et al., 1993) and contained slightly more Syt I reactivity as measured by fluorescence intensity (supplemental Fig. S4, available at www.jneurosci.org as supplemental material). NMJs were also labeled with the monoclonal antibody nc82, which recognizes the active zone component BRP (Kittel et al., 2006; Wagh et al., 2006; Hofbauer et al., 2009). The density and number of BRP puncta per bouton in *impβ11* mutant NMJs were

Table 1. Quantification of glutamate receptors in third instar control and *imp-β11* larvae

Genotype	GluRIIA	GluRIIB	GluRIIC
Control	0.63 ± 0.030	0.54 ± 0.018	0.52 ± 0.025
imp-β11^{70}/Df	0.65 ± 0.036	0.54 ± 0.039	0.58 ± 0.030

Quantification of the number of glutamate receptor puncta at synaptic boutons on muscle 4 divided by the synaptic surface area as determined by HRP staining. $n > 12$ NMJs for both genotypes.

unchanged (Fig. 4*B*) (control, 0.70 ± 0.029 puncta/μm^2; *impβ11^{70}/Df*, 0.79 ± 0.035 puncta/μm^2; $n \geq 13$ for both genotypes). However, because there were fewer boutons per NMJ, there was a net decrease in total active zone number, and this loss of release sites was likely an important factor in the reduction in synaptic strength.

The impairment in mEJP amplitude suggested that there might have been an alteration in postsynaptic glutamate receptors (Petersen et al., 1997; DiAntonio et al., 1999; Marrus et al., 2004). To examine receptor density and localization, we therefore undertook immunolabeling for GluRIIA, GluRIIB, and GluRIIC, but all appeared normal in the *impβ11* mutant NMJs. The intensity of the labeling was unchanged and clusters of receptors properly localized beneath active zones (Fig. 4*C*, Table 1). Thus, within the reduced synaptic arbor of *impβ11* mutants, each bouton retained active zones with synaptic vesicles and faced a postsynaptic membrane with properly clustered glutamate receptors.

Reduced pMAD at *impβ11* NMJs

The quantitative reduction in bouton number suggested that *impβ11* mutants may be defective in one of several signaling pathways known to modulate the development of this synapse (Collins and DiAntonio, 2007). These include the BMP pathway, the Wnt pathway, and the mitogen-activated protein kinase pathways (Marqués, 2005; Collins et al., 2006; Speese and Budnik, 2007). In particular, disruption of the BMP pathway reduces bouton number and EJP amplitude, and thus resembles the *impβ11* phenotype. At the NMJ, secretion of the ligand glass bottom boat (Gbb) from the muscle activates the BMP pathway by causing the receptor complex composed of Wit, Tkv, and Saxophone (Sax) to phosphorylate the signaling molecule MAD (Keshishian and Kim, 2004). The C-terminally phosphorylated form, pMAD, is abundant both at the NMJ and in motor neuron nuclei, and therefore may act locally or by retrogradely translocating to the nucleus (Allan et al., 2003; McCabe et al., 2003; Marqués, 2005). The pathway is likely to function bidirectionally, with some pMAD generated in the muscle as well as in the nerve terminals (Dudu et al., 2006; Collins and DiAntonio, 2007). Recently, several studies have identified proteins that interact with and modulate the BMP pathway at the *Drosophila* NMJ (Wang et al., 2007; O'Connor-Giles et al., 2008; Merino et al., 2009). We therefore examined the distribution of pMAD as a readout of the activity of this pathway and its potential interaction with importin-β11.

In control animals, pMAD immunoreactivity (Persson et al., 1998) was present both at the NMJ, overlapping with the neuronal marker HRP, and in motoneuron nuclei (Fig. 4*D*,*F*). In *impβ11* mutants, pMAD still accumulated in motor neuron nuclei (Fig. 4*G*), but synaptic pMAD was markedly reduced at the NMJs of all muscles (Fig. 4*E*; quantified in supplemental Fig. S5, available at www.jneurosci.org as supplemental material). This phenotype is distinct from that of *wit* mutants, which lose both nuclear (Marqués et al., 2002) and synaptic pMAD (supplemental Fig. S6, available at www.jneurosci.org as supplemental material).

Like the localization of pMAD itself (Dudu et al., 2006; Collins and DiAntonio, 2007), the reduction in synaptic pMAD in *impβ11* appeared to have both presynaptic and postsynaptic components. Restoration of importin-β11 expression to the nervous system, by means of *elav-GAL4* or ubiquitous expression with *da-GAL4*, was sufficient to restore pMAD immunolabeling to the nerve terminals to control levels (Fig. 4*H*,*I*; quantified in supplemental Fig. S5, available at www.jneurosci.org as supplemental material). Expression of the transgene in muscle with *G14-GAL4*, however, was also capable of increasing pMAD immunoreactivity to the mutant NMJ, but to a lesser extent than neuronal or ubiquitous rescue (Fig. 4*J*; quantified in supplemental Fig. S5, available at www.jneurosci.org as supplemental material). The NMJ phenotypes of *MAD* mutants and other genes in the BMP signaling pathway are known to arise from presynaptic requirements for this pathway (Aberle et al., 2002; McCabe et al., 2004). Because bouton number, EJP amplitude, and pMAD phenotypes of *impβ11* were rescued to control values with presynaptic restoration of importin-β11, loss of specifically presynaptic pMAD is also the most likely explanation of the anatomical and electrophysiological defects in *impβ11*.

BMP pathway components are present at *impβ11* mutant NMJs

Importins, by mediating the nuclear import of transcription factors, might be required for the expression of a component of the BMP pathway, and thus influence the production of pMAD. We therefore investigated whether the loss of synaptic pMAD resulted from the loss of a component of the pathway. To test whether low Gbb production caused the reduced pMAD, we expressed a *UAS-gbb* transgene in muscle and determined whether it would restore pMAD to the mutant NMJ. Although expression of the *gbb* transgene increased nuclear pMAD in muscle, thereby confirming the efficacy of the transgene, pMAD was not restored to *impβ11* mutant NMJs (Fig. 5*A–E*). Thus, loss of Gbb is unlikely to explain the loss of pMAD in *impβ11* mutants. Reductions in synaptic pMAD might also have arisen because of the absence of the receptors or MAD itself. We addressed these possibilities by comparing the immunolocalization of MAD, Wit, and Tkv. MAD and Wit labeling in control NMJs were detected both within boutons and at their margins; the latter staining likely represented both presynaptic and postsynaptic pools. Anti-Tkv clearly labeled both the presynaptic and postsynaptic compartments. Similar patterns of immunolabeling for MAD, Wit, and Tkv were also observed in *impβ11* NMJs (Fig. 5*F–K*), indicating that the loss of pMAD from the NMJ was not caused by the absence of the substrate or receptors from the synapse. Because anti-MAD and anti-Wit only dimly labeled some boutons, we used additional methods to examine the presence of each protein in *impβ11*. For Wit, we examined the VNC where the receptor had previously been localized (Aberle et al., 2002) and found that anti-Wit immunoreactivity was not markedly altered in *impβ11* (supplemental Fig. S7*A*,*B*, available at www.jneurosci.org as supplemental material). As an additional method to test whether a lack of MAD could account for the loss of pMAD, we expressed a *UAS-GFP-MAD* transgene in the nervous system of *impβ11* mutant larvae with *elav-GAL4*. This transgene can functionally replace the endogenous protein in *MAD* mutants (Dudu et al., 2006). Expression of *UAS-GFP-MAD*, however, did not rescue the pMAD defect in *impβ11*, further indicating that the mutant defect was not attributable to a reduction in the substrate MAD

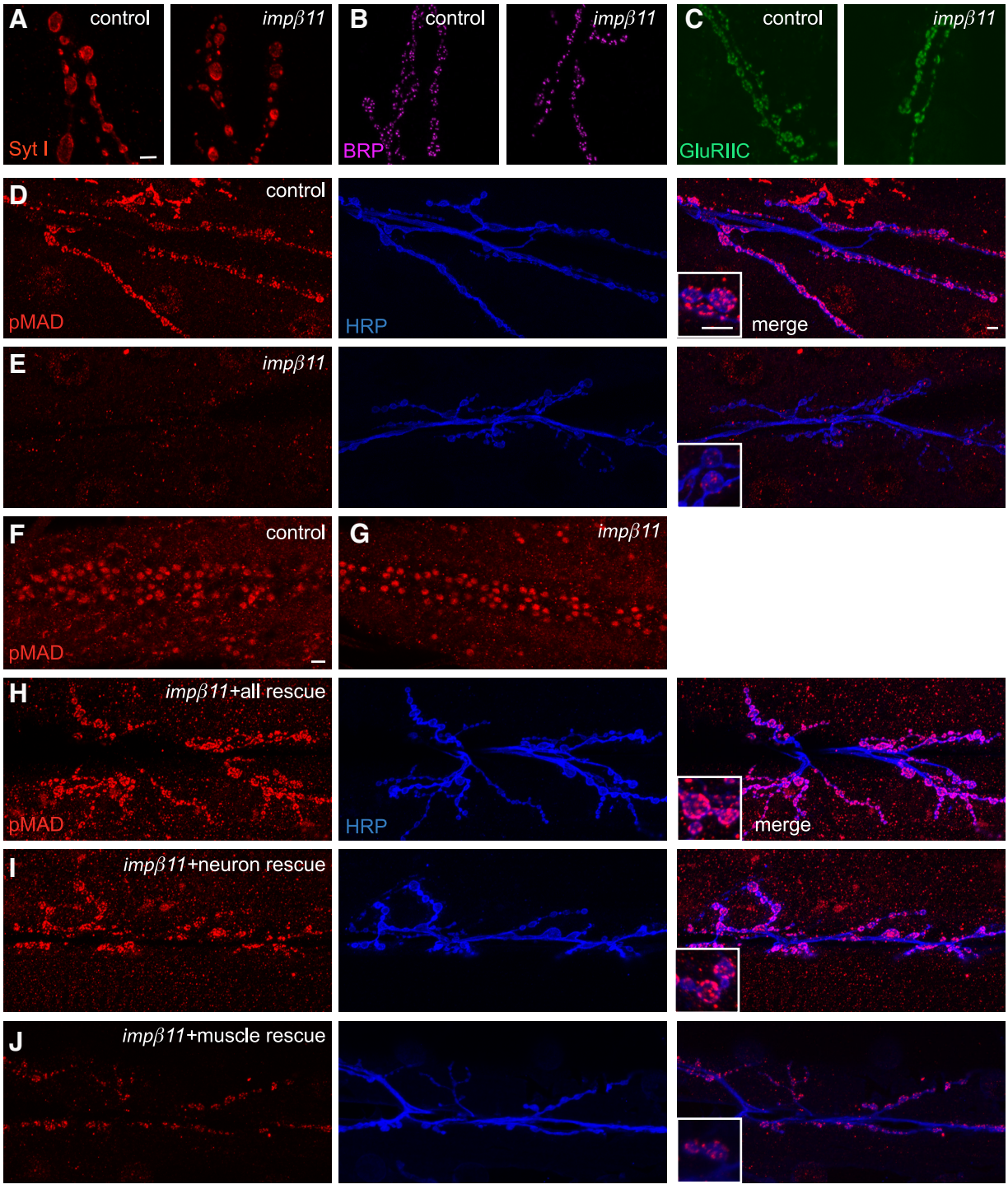

Figure 4. Synaptic pMAD is reduced in *impβ11* mutants but other synaptic proteins appear normal. ***A–C***, Representative confocal images of third-instar NMJs stained with antibodies to synaptic proteins to localize synaptic vesicles (with anti-Syt I; ***A***, red), active zones (with anti-BRP; ***B***, magenta), and glutamate receptors (with anti-GluRIIC; ***C***, green) to control and *impβ11* mutant terminals. These proteins appeared unaltered at the *impβ11* mutant NMJs. ***D***, ***E***, Immunoreactivity for pMAD (red) at control (***D***) and mutant (***E***) NMJs whose neurons were marked with anti-HRP (blue). *impβ11* mutants consistently had low levels of pMAD at the NMJ. Insets show higher magnifications of the representative boutons. ***F***, ***G***, Nuclear pMAD was detected in both control and mutant VNCs including motor neurons. ***H–J***, Expression of *UAS-impβ11-eGFP* in the *impβ11* mutant background in all cells (***H***) or in neurons (***I***) rescued pMAD immunoreactivity (red) to control levels, but expression in muscle (***J***) only slightly increased pMAD staining above the levels in the mutant. Scale bars, 10 μm. Genotypes are as follows: control (*y,w;FRT42D*), *impβ11* (*FRT42D, impβ11^{70}/Df*), all rescue (*FRT42D, impβ11^{70}/Df; da-GAL4/UAS-impβ11-eGFP*), neuron rescue (*FRT42D, impβ11^{70}/Df; elav-GAL4/UAS-impβ11-eGFP*), muscle rescue (*FRT42D, impβ11^{70}, G14-GAL4/Df; UAS-impβ11-eGFP/+*).

(supplemental Fig. S7*C–F*, available at www.jneurosci.org as supplemental material). Thus, in *impβ11* mutants, the reduction in synaptic pMAD could not be explained by a loss of the ligand, receptors, or MAD itself.

To determine whether other functions that rely on BMP signaling were intact in *impβ11* mutants, philanthotoxin-induced synaptic homeostasis was examined. This phenomenon entails a compensatory presynaptic increase in quantal content after the

Table 2. Genetic interactions between *impβ11* and BMP components

Genotype	Mean bouton no.	% of control
Control	0.88 ± 0.048	100
$imp\beta11^{70}$/+	0.86 ± 0.033	98
Df/+	0.88 ± 0.028	100
$imp\beta11^{70}$/*Df*	0.62 ± 0.044	70
mad^{10}/+	0.92 ± 0.046	104
wit^{A12}/+	0.87 ± 0.057	99
wit^{HA1}/+	0.92 ± 0.040	104
wit^{A12}/wit^{B11}	0.42 ± 0.047	48
$imp\beta11^{70}/mad^{10}$	0.75 ± 0.020	85
$imp\beta11^{70}$/+; wit^{A12}/+	0.71 ± 0.020	81
$imp\beta11^{70}$/+; wit^{HA1}/+	0.76 ± 0.025	86
$imp\beta11^{70}$/+; $n\text{-}syb^{F\text{-}33R}$/+	0.85 ± 0.048	96
$imp\beta11^{70}$/*UAS-wit*; wit^{HA1}/*elav-GAL4*	0.92 ± 0.049	104
$imp\beta11^{70}$/*Df*+ *act R* neuron rescue	0.98 ± 0.040	111
$imp\beta11^{70}$/*Df*+ *act R* muscle rescue	0.70 ± 0.026	80

Bouton numbers per 1000 μm^2 muscle surface area are displayed as mean values and percentages of control. *p* values and full genotypes are noted in the figure legends.

acute blockade of transmission at third-instar NMJs by means of the use-dependent glutamate receptor antagonist PhTx (Frank et al., 2006). This process fails in *gbb* and *wit* mutant larvae, and the BMP pathway is therefore thought to have a permissive role, although not necessarily to be acutely involved in the upregulation of transmission (Goold and Davis, 2007). To examine this phenomenon, both control and *impβ11* mutant third-instar larvae were exposed to PhTx for 10 min and compared with preparations of the same genotypes mock-treated with saline. In both mutants and controls, PhTx decreased mEJP amplitude, whereas EJP amplitude remained unchanged (supplemental Fig. S8, available at www.jneurosci.org as supplemental material). Thus, the mechanisms governing the homeostatic increase in quantal content remained operational in the *impβ11* larvae, despite the lack of pMAD at these NMJs. Therefore, the local pool of pMAD at the NMJ may not be required acutely for PhTx-induced synaptic homeostasis. Because block of retrograde transport of pMAD has been shown to hinder PhTx-induced homeostasis (Goold and Davis, 2007), nuclear pMAD is most likely responsible for permitting this form of plasticity. Thus, although pMAD is generated in the periphery by BMP signaling, it does not need to remain resident in the terminals for homeostasis to be enabled.

Genetic interaction of *impβ11* and the BMP pathway

The similarity between published BMP pathway mutants and those associated with loss of importin-β11 function, as well as the observed reduction in pMAD at *impβ11* terminals, suggested that importin-β11 and the BMP pathway interacted to regulate the development of the synapse. To test this hypothesis, we examined genetic interactions between *impβ11* and the BMP pathway. Although mutations in *impβ11* and BMP pathway components each reduce bouton counts, this phenotype is recessive; heterozygotes for these alleles are normal (Figs. 3B, 6*A*; Table 2). In contrast, larvae made heterozygous for both $imp\beta11^{70}$ and either a null allele of *MAD* (MAD^{10}) (Sekelsky et al., 1995), a *wit* null allele (wit^{A12}) (Marqués et al., 2002), or a hypomorphic allele of *wit* (wit^{HA1}) (Aberle et al., 2002) had significantly fewer boutons than either wild-type or each heterozygous alleles alone (Fig. 6*A*, Table 2). These genetic interactions were specific for mutations in the BMP pathway; larvae heterozygous for *impβ11* and the synaptic transmission mutant *neuronal synaptobrevin* (*n-syb*) (Deitcher et al., 1998) had normal synaptic arbors. Neuronal expression of *UAS-wit* was able to reverse the reduction in bouton number in $imp\beta11^{70}$/+; wit^{HA1}/+ larvae (Fig. 6*A*, Table 2). The interaction between importin-β11 and BMP components is therefore likely to occur presynaptically and, consistent with a role for importin-β11 in BMP signaling, resembles the genetic interactions of other heterozygous combinations of mutations in the BMP pathway (McCabe et al., 2004).

Because BMP pathway mutants resemble *impβ11* mutant alleles, reducing both bouton number and synaptic strength, loss of pMAD could explain these *impβ11* phenotypes. Restoration of synaptic pMAD in *impβ11* null larvae would then be predicted to rescue the phenotypes. To this end, we introduced into motor neurons expression of constitutively active receptors with the driver *OK6-GAL4* (Aberle et al., 2002) and *UAS-*tkv^{act}, sax^{act} transgenes (Holley et al., 1996; Hoodless et al., 1996). This expression, but not postsynaptic expression (*G14-GAL4*), restored pMAD to *impβ11* mutant terminals, a finding consistent with our conclusion that an absence of MAD cannot account for the loss of pMAD in *impβ11* mutants (Fig. 6*B–F*). Concomitant with pMAD restoration, expression of the activated receptors in motor neurons also rescued the bouton number and EJP phenotypes in *impβ11* to control levels, although mEJP frequency was not rescued (Fig. 6*A*, *G–J*, Table 2). Expression of the activated receptors in muscle (*G14-GAL4*) did not rescue any of the phenotypes (Fig. 6*A*, *G–J*, Table 2). In control larvae, expression of the activated receptors in motor neurons did not change pMAD levels or the electrophysiological profile at the NMJ (Fig. 6*C*,*G–J*). Thus, restoring the presynaptic pool of pMAD was sufficient for normal bouton number and EJP amplitude. Moreover, the rescue of these phenotypes in the *impβ11* mutants cannot be attributed to a simple addition of a *UAS-*tkv^{act}, sax^{act}-induced increase and an *impβ11*-induced decrease as there is no gain-of-function phenotype, but rather to overcoming a particular deficit in pMAD signaling in the *impβ11* genotype.

Reduction of retrograde transport restores *impβ11* phenotypes

The levels of pMAD in nerve terminals may also be controlled by the rate at which it, or a component of the pathway, is transported away from the terminal to the nucleus or for degradation. Inhibiting the retrograde motor dynein by expression of p150-Glued blocks retrograde BMP signaling and reduces nuclear pMAD with consequent effects on NMJ development (Eaton et al., 2002; Allan et al., 2003; Marqués et al., 2003; McCabe et al., 2003). The dynein motor may transport pMAD itself or another signaling component required for pMAD production or maintenance. Therefore, we hypothesized that the structural and functional phenotypes of *impβ11* might also be rescued by inhibiting retrograde transport. Overexpression of dynamitin inhibits transport by destabilizing the dynein motor complex (Duncan and Warrior, 2002; Melkonian et al., 2007), but to a lesser extent than p150-Glued expression. When *UAS-dynamitin* was expressed in motor neurons with the *OK6-GAL4* driver in a wild-type background, pMAD immunoreactivity at the NMJ was similar to control levels (Fig. 7*A*,*B*), and nuclear pMAD showed no obvious reduction (Fig. 7*E*,*F*). Bouton number and electrophysiological properties were likewise unchanged (Fig. 7*G–K*). When *UAS-dynamitin* was expressed in the *impβ11* mutant background, however, the loss of synaptic pMAD was prevented (Fig. 7*C*,*D*). These findings confirmed that the elements of the BMP pathway in the terminal were preserved and at least partially active in the *impβ11* larvae and suggested that the reduction in synaptic pMAD might arise

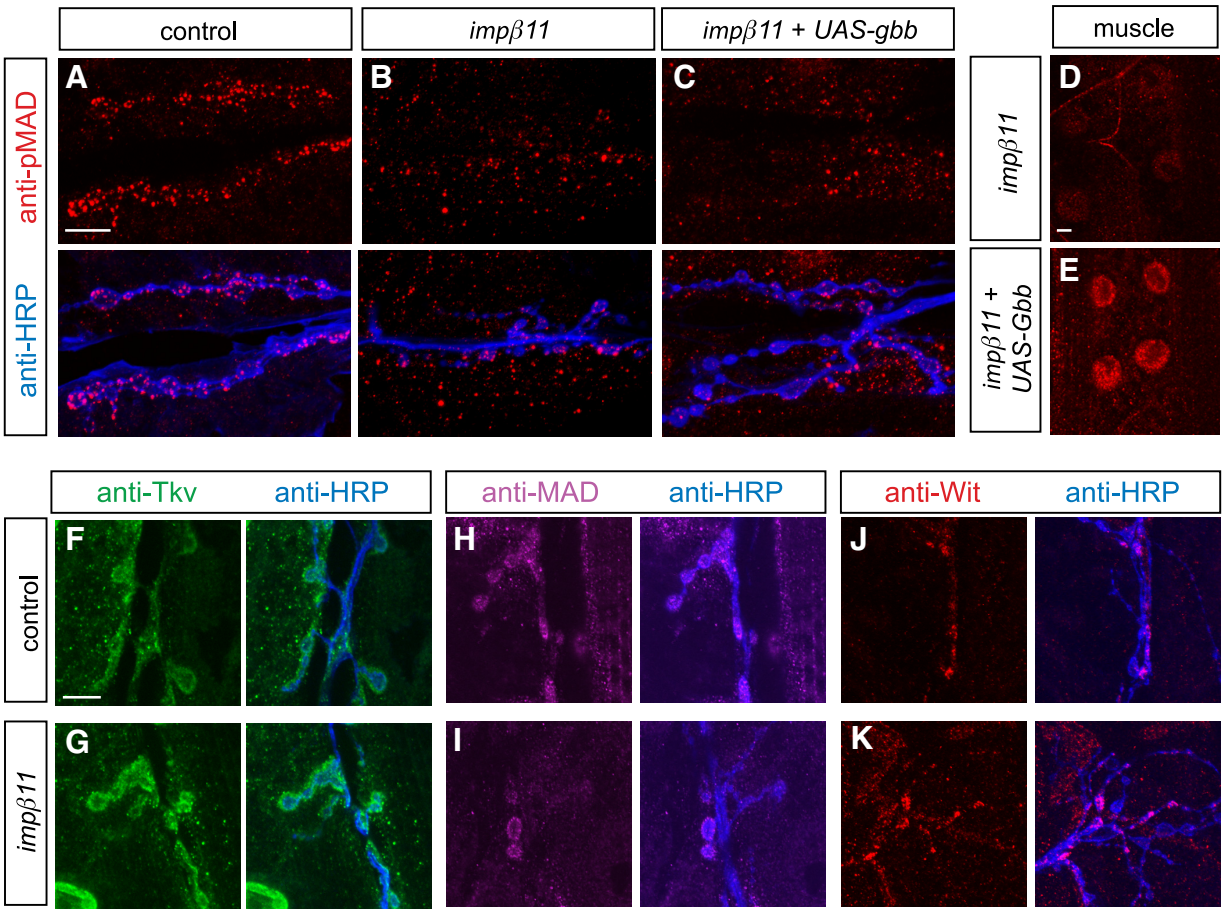

Figure 5. BMP pathway components are present at *impβ11* NMJs. ***A–C***, Representative confocal images of third-instar NMJs stained with anti-pMAD (red) and anti-HRP (blue). ***A***, ***B***, pMAD was detected at control NMJs (***A***) but was reduced at mutant NMJs (***B***). ***C–E***, Overexpression of *UAS-gbb* in muscle did not restore pMAD to mutant terminals, but did increase pMAD in muscle nuclei (***D***, ***E***). ***F–K***, Representative confocal images of NMJs from control and *impβ11* larvae immunostained for anti-HRP (blue) and components of the BMP pathway. ***F***, ***G***, In control and mutant NMJs, the BMP receptor Tkv (green) was visible both within and around the boutons. ***H–K***, The substrate of BMP receptors, MAD (magenta), and the receptor Wit (red) were present at both mutant and control synapses. Scale bars, 10 μm. Genotypes are as follows: control (*y,w;FRT42D*), *impβ11* (*FRT42D,impβ11^{70}/Df*), *impβ11 + UAS-gbb* (*w; FRT42D, impβ11^{70}, G14-GAL4/Df; UAS-gbb*).

from an excess of retrograde transport away from the terminal. Coincident with pMAD restoration to the mutant terminal, EJP amplitude, mEJP frequency, quantal content, and bouton number were rescued to control values (Fig. 7*G–K*). No defect in mEJP amplitude was detected in *impβ11$^{70/70}$* larvae (Fig. 7*I*). These data indicate that restriction of retrograde transport is sufficient to reverse *impβ11* phenotypes and suggest that importin-β11 promotes or stabilizes pMAD localization to the NMJ, which is in turn required for synapse formation and transmission.

Discussion

Drosophila mutants have allowed us to examine, *in vivo*, importin-β11 and uncover its synaptic function and relationship with the BMP pathway. Loss of importin-β11 causes specific developmental and functional defects: motor neurons develop fewer boutons, and EJP amplitudes are 40% lower than controls.

Importin-βs are structurally diverse; they share a small N-terminal Ran-binding domain but the remaining C terminus of each is unique and allows for substrate specificity and functional diversity (Mosammaparast and Pemberton, 2004). This diversity extends from interactions with nucleoporins to functions in the cell periphery or neuronal synapses (James et al., 2007; Ting et al., 2007). At these locations, they can begin the process of movement to the nucleus but also have additional functions (Harel and Forbes, 2004; Otis et al., 2006; Perry and Fainzilber, 2009).

The functional specificity of importins is illustrated by the *impβ11* phenotypes, phenotypes that are not shared by other known importin mutants and arise only in a subset of tissues. For example, mutations in *imp13* do not alter NMJ bouton number and enhance rather than decrease neurotransmitter release (Giagtzoglou et al., 2009). Similarly, mutations in *impα3* lead to errors in the axonal projections of photoreceptors, a defect not seen in *impβ11* (Ting et al., 2007; T. Herman, personal communication). Thus, the loss of this importin does not grossly disrupt all nuclear import, but rather causes a restricted and distinct phenotype. Homozygous null *impβ11* clones in the eye primordium undergo cell division and differentiation and give rise to outwardly normal photoreceptors with correct axonal projections, but have defects in synaptic transmission. At the NMJ, the phenotype is similarly restricted to a synaptic defect with no apparent compromise in motor neuron viability, differentiation, or axon guidance.

The NMJ defects in *impβ11* null larvae are partial reductions in bouton number and synaptic strength rather than a complete failure of development or transmission. The electrophysiological defect in photoreceptors is less understood, but sufficient to prevent phototaxis. In addition to these defects, some neuronal sub-

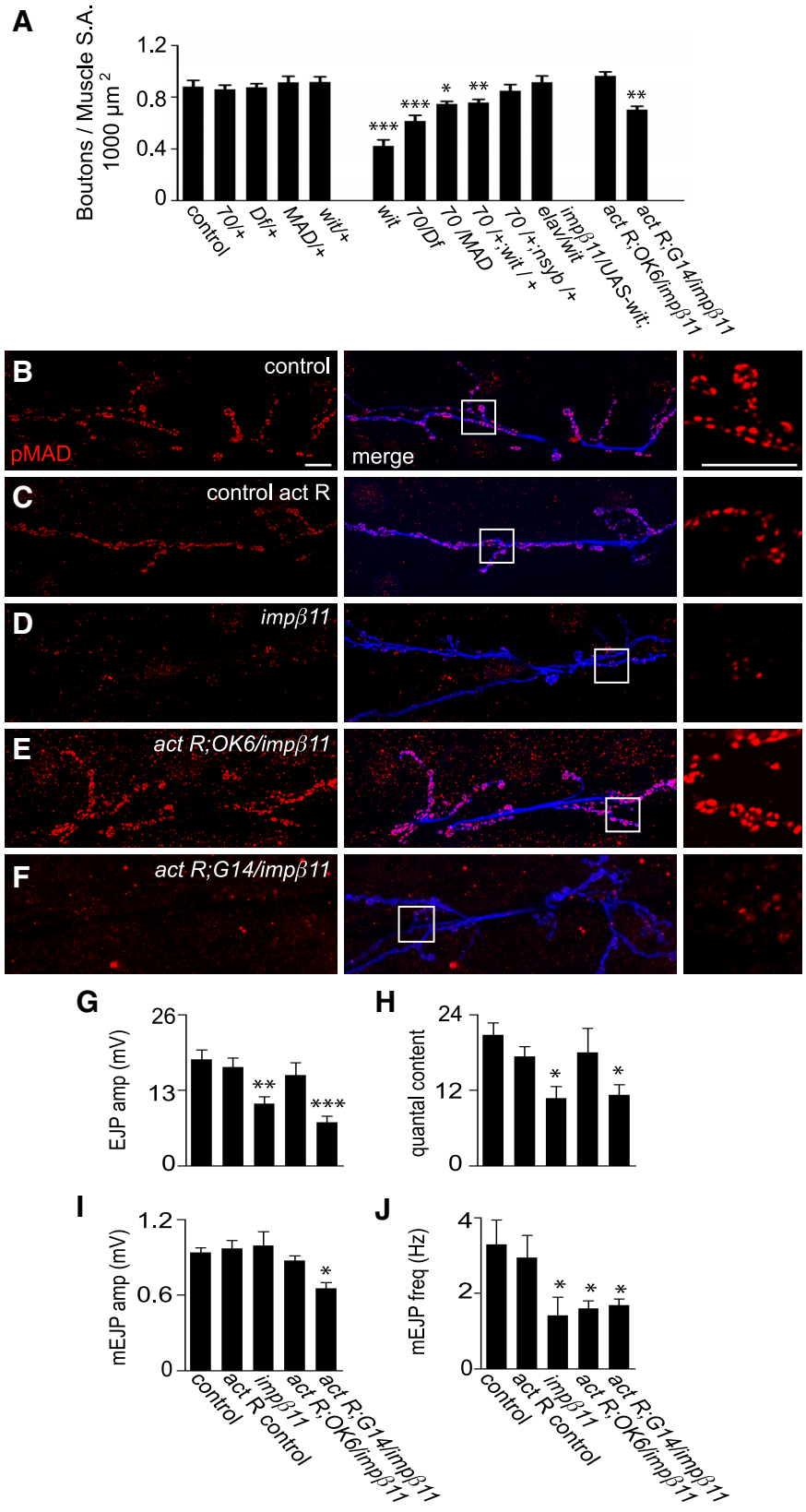

Figure 6. Genetic interaction of *impβ11* and the BMP pathway. ***A***, BMP pathway mutants and *impβ11* interact to form fewer synaptic boutons on muscles 6 and 7. Bouton counts were normal in heterozygotes of $impβ11^{70}$ or the indicated alleles of BMP pathway mutants but reduced in larvae heterozygous for both $impβ11^{70}$ and either MAD^{10} or wit^{HA1}, an interaction not seen with $n\text{-}syb^{F\text{-}33R}$. Bouton number was rescued by presynaptic expression of *UAS-wit* in $impβ11^{70}$; wit^{HA1} transheterozygotes. In addition, neuronal (but not muscle) expression of constitutively activated BMP receptors ($UAS\text{-}tkv^{act}$, sax^{act}) restored bouton number in an *impβ11* mutant background. ***B–F***, Representative confocal images of anti-pMAD (red) and anti-HRP (blue) immunoreactivity to illustrate the effects of the constitutively activated BMP receptors on pMAD levels. Scale bars, 10 μm. In control larvae, the activated receptors driven in motor neurons did not appreciably increase pMAD (***C***), but in *impβ11* larvae pMAD levels were restored (***E***). When activated receptors were expressed in *impβ11* muscle, pMAD staining was not restored (***F***). ***G–J***, EJP amplitude and quantal content, but not mini frequency, were restored to control levels by the activated BMP receptors expressed in motor neurons but not in muscle. Recordings were conducted in 0.6 mM Ca^{2+} HL3; $n \geq 6$ for each genotype. $^{*}p < 0.05$; $^{**}p < 0.001$; $^{***}p < 0.0001$ compared to control. Genotypes are as follows: control (*y,w; FRT42D*), 70/+ (*w;FRT42D, impβ11*^{70}/+), MAD/+ (MAD^{10}/+), wit/+ (wit^{HA1}/+), wit (wit^{A12}/wit^{B11}), 70/Df (*FRT42D, impβ11*^{70}/ *Df*), 70/MAD (*FRT42D, impβ11*^{70}/ mad^{10}), 70/+;wit/+ (*FRT42D, impβ11*^{70}/+; wit^{HA1}/+), 70/+;n-syb/+ (*FRT42D, impβ11*^{70}/+; $n\text{-}syb^{F\text{-}33R}$/+), 70/UAS-wit;elav/wit (*FRT42D, impβ11*^{70}/*UAS-wit;* elav-GAL4/wit^{HA1}), control act R (*UAS-tkv*^{act}, *UAS-sax*^{act}; *OK6-GAL4/+*), act R;*OK6/ impβ11* (*UAS-tkv*^{act}, *UAS-sax*^{act}; *FRT42D, impβ11*^{70}, *OK6-GAL4/Df*), act R;*G14/ impβ11* (*UAS-tkv*^{act}, *UAS-sax*^{act}; *FRT42D, impβ11*^{70},*G14-GAL4/Df*).

types must be more drastically impaired than motor neurons because neuronal importin-β11 is essential for viability. Additional nonneuronal functions are indicated by the failure of oocyte maturation in mutant germline clones, the expression of importin-β11 in early embryos, and importin-β11 immunoreactivity at the nuclear envelope in muscle. Although importin-β11 is expressed in both nerve and muscle, the reduction in bouton number and synaptic strength in *impβ11* null larvae results primarily from a loss of neuronal importin-β11 and can be restored by neuronal expression of importin-β11. Other aspects of NMJ development, however, are dependent on importin-β11 in muscle (T. J. Mosca and T. L. Schwarz, unpublished observation). Thus, importin-β11 functions are both diverse and highly selective.

Of the many factors contributing to NMJ development and function (Keshishian et al., 1996; Collins and DiAntonio, 2007), importin-β11 action appears particularly connected to the BMP pathway. The evidence for this connection is fourfold. (1) At *impβ11* NMJs, pMAD is markedly reduced. Neuronal expression of an *impβ11* transgene restores pMAD levels in parallel with restoration of bouton number and EJP amplitude. The decrease in pMAD is not part of a widespread loss of synaptic proteins as FasII, Futsch, Syt I, BRP, GluRIIA, GluRIIB, and GluRIIC are not lacking. (2) Mutations in the BMP pathway, including mutations in *MAD*, result in *impβ11*-like phenotypes: fewer boutons and smaller EJPs (Marqués, 2005). (3) Mutations in *impβ11* interact genetically with mutations in *MAD* and *wit*; heterozygous mutations that are recessive

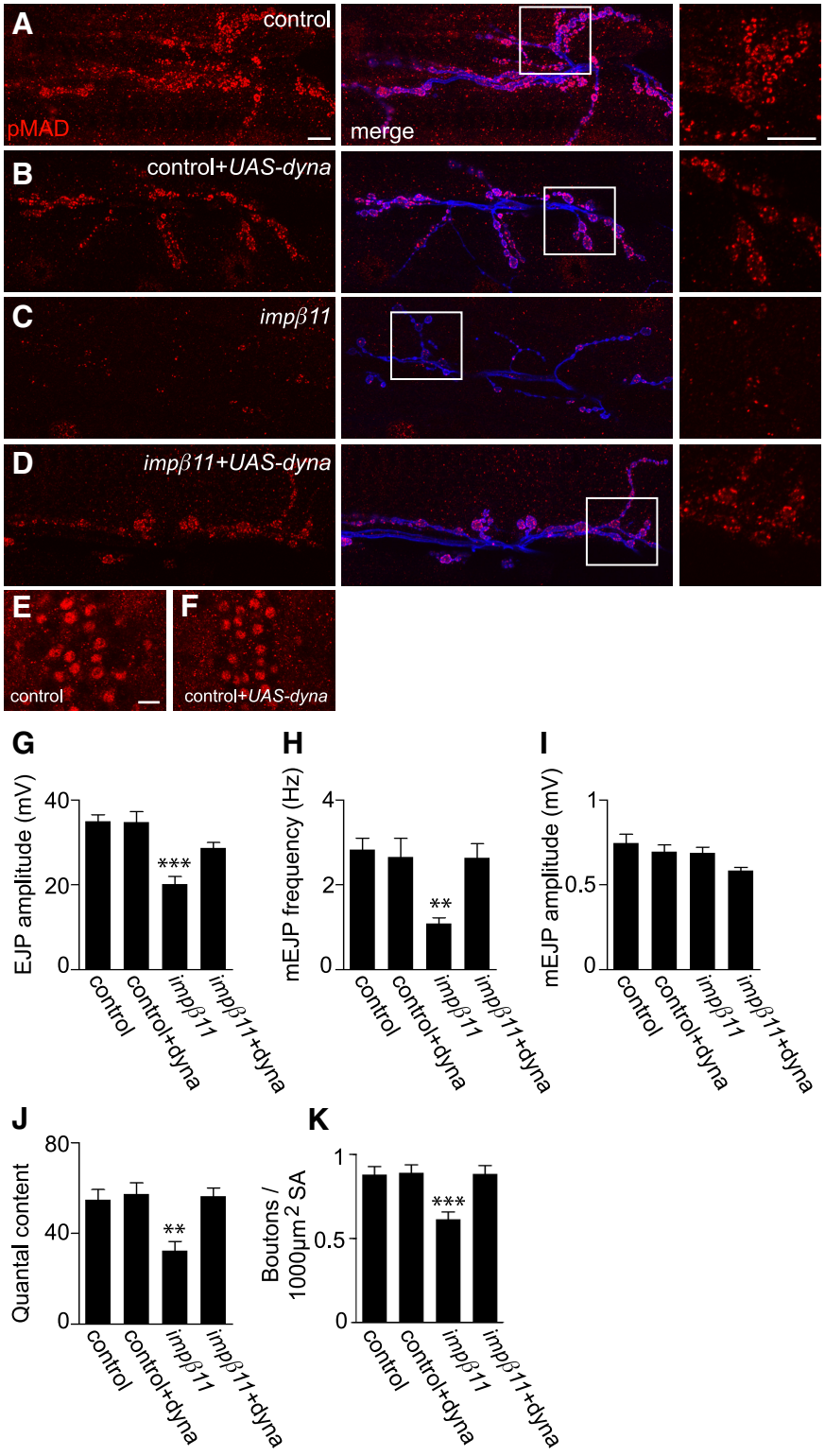

Figure 7. Overexpression of dynamitin can reverse *impβ11* phenotypes. ***A–D***, Representative confocal images of NMJs immunostained with anti-pMAD (red) and anti-HRP (blue). Scale bars, 10 μm. ***B–F***, Motor neuron expression of *UAS-dynamitin* in a control background did not detectably alter pMAD levels at the NMJ or in motor neuron nuclei (***B***, ***F***); when compared with control (***A***, ***E***); however, pMAD was restored to *impβ11* NMJs (***C***, ***D***). ***G–J***, Expression of dynamitin in a control background did not alter EJP amplitude, mEJP frequency, or quantal content, but reversed the reduction in those parameters in *impβ11* mutants (EJP amplitude: control, 35.0 ± 1.56 mV; control+dyna, 34.8 ± 2.45 mV; *impβ11*, 20.1 ± 1.84 mV; *impβ11*+dyna, 28.7 ± 1.30 mV; mEJP frequency: control, 2.83 ± 0.274 Hz; control+dyna, 2.66 ± 0.441 Hz; *impβ11*, 1.08 ± 0.142 Hz; *impβ11*+dyna, 2.64 ± 0.331 Hz; quantal content: control, 54.8 ± 4.55; control+dyna, 57.4 ± 4.90; *impβ11*, 32.5 ± 4.10; *impβ11*+dyna, 56.3 ± 3.86). ***I***, mEJP amplitude was normal in all genotypes. ***K***, Similarly, dynamitin overexpression in a control background did not alter bouton number but in *impβ11* restored bouton number to control values. $^{**}p < 0.001$; $^{***}p < 0.0001$ compared to control; $n \geq 8$ animals for each genotype. Genotypes are as follows: control (*y,w; FRT42D*), control+dyna (*UAS-dynamitin/OK6-GAL4*), *impβ11* (*w;FRT42D, impβ11$^{70/70}$*), *impβ11+dyna* (*UAS-dynamitin, FRT42D, impβ11^{70}/FRT42D, impβ11^{70}, OK6-GAL4*).

independently interact to reduce bouton number when combined. These genetic interactions with *impβ11* are comparable to those between established BMP-pathway members (McCabe et al., 2004). (4) Restoration of synaptic pMAD levels in *impβ11* mutants either by constitutively activated BMP receptors or impaired retrograde transport also rescues the bouton and EJP phenotypes.

These data suggest that, under normal conditions, importin-β11 permits a synaptic pool of pMAD to exist and that this pool of presynaptic pMAD is required for normal NMJ structure and function. Although SMADs chiefly act as transcription factors, there is growing precedent for alternative posttranscriptional functions (Davis et al., 2008; Hoover and Kubalak, 2008; Tang et al., 2008). A local, synaptic function of pMAD presently provides the simplest explanation of the correlation of the *impβ11* null phenotypes and local pMAD levels. The mechanism underlying the reduction in synaptic pMAD, however, remains unknown. We have been unable to detect by immunoprecipitation a direct interaction between importin-β11 and several members of the BMP pathway (data not shown). Moreover, the essential elements of the pathway, Wit, Tkv, and MAD itself, remain in the mutant terminals, and overexpression of GFP-MAD neither restores pMAD levels nor alleviates the *impβ11* phenotype. Therefore, a failure to transcribe or traffic these proteins cannot account for the loss of pMAD. In contrast, overactivation of the receptors by constitutively activated *tkv* and *sax* overcomes the *impβ11* phenotype. A standard genetic explanation of this rescue by activated receptors would be that the disruption of the pathway is upstream of the receptor, in this case loss of Gbb secretion by the muscle. This is unlikely to explain the *impβ11* phenotype, however, because importin-β11 is required in the nervous system, not muscle, for maintaining normal pMAD levels. Furthermore, overexpression of Gbb does not suppress the loss of pMAD at *impβ11* synapses. Thus, fundamentals of the BMP pathway, the receptors, and their ligand and substrate, are intact at the *impβ11* NMJ. Indeed, the continued function-

ing of the pathway is suggested by the presence of nuclear pMAD in the motor neurons and by the occurrence of homeostatic compensation to PhTx at the synapse, a process that fails in mutations of the BMP pathway (Goold and Davis, 2007). Instead, the loss of synaptic pMAD in *impβ11* may likely arise from a modulation of this pathway that causes pMAD to be lost locally from the terminals while keeping intact the pathway for pMAD production and nuclear localization.

Excess retrograde transport of pMAD from the NMJ might plausibly explain pMAD loss in *impβ11*. Importin-β11 might inhibit, either directly or indirectly, retrograde transport of pMAD from terminals, and thereby retain a pool of synaptic pMAD for local functions. This hypothesis is consistent with an intact BMP pathway, persistent nuclear pMAD in motor neurons, and selective loss of synaptic pMAD. Synaptic receptors are needed for nuclear pMAD in a pathway that depends on retrograde transport (Marqués, 2005). Although we do not see increased nuclear pMAD in mutant motor neurons, increased transport out of the terminals need not cause a detectable increase in the nuclear pool. pMAD-dependent transcriptional regulation likely promotes synapse development, probably as a permissive signal for NMJ growth (Collins and DiAntonio, 2007; Goold and Davis, 2007). Synaptic pMAD may instead maintain or remodel the NMJ more subtly. This difference can explain why mutations in *wit*, which reduce pMAD in both terminals and nuclei, cause stronger synaptic defects than *impβ11* (Aberle et al., 2002; Marqués et al., 2002). Other possible explanations of the pMAD phenotype include a role for importin-β11 in protecting the synaptic pool from dephosphorylation or degradation, or a modulatory effect of the importin on the basal activation of the BMP receptors. In addition, we cannot rule out subtle alterations in nuclear pMAD caused by potential redundancy of importin-β11 with other importins (Xu et al., 2007) or effects of maternally contributed importin-β11.

A defect in nuclear import might indirectly, perhaps through transcriptional changes, control synaptic pMAD levels. Such a mechanism would be consistent with importin-β11 localization at neuronal nuclear pores and with the canonical function of importins. However, because importin-β11-eGFP localizes to the NMJ and other importins occur at synapses (Thompson et al., 2004; Ting et al., 2007), importin-β11 might instead act synaptically to modulate pMAD. Whether acting locally, at the nuclear pore, or both, our data reveal a potentially novel function for an importin in regulating BMP signaling. Because many other factors and pathways interact with BMP signaling (von Bubnoff and Cho, 2001; Keshishian and Kim, 2004; Collins and DiAntonio, 2007), there are many potential targets for further investigation of importin-β11 mechanisms.

Although importins have primarily been examined at the nuclear pore, they also undergo long-distance translocations in the cytoplasm that can be important for signal transduction (Guillemain et al., 2002; James et al., 2007). These functions are of particular interest in the nervous system and include synapse-to-nucleus shuttling where they are implicated in synaptic plasticity, axonal regeneration, and axonal targeting (Otis et al., 2006; Ting et al., 2007; Perry and Fainzilber, 2009). With the characterization of *Drosophila impβ11*, the regulation of synaptic development and strength can be added to the repertoire of importin-dependent functions, whereas the phenotype of the mutations serves to highlight the functional selectivity of an individual importin.

References

Aberle H, Haghighi AP, Fetter RD, McCabe BD, Magalhaes TR, Goodman CS (2002) Wishful thinking encodes a BMP type II receptor that regulates synaptic growth in *Drosophila*. Neuron 33:545–558.

Allan DW, St Pierre SE, Miguel-Aliaga I, Thor S (2003) Specification of neuropeptide cell identity by the integration of retrograde BMP signaling and a combinatorial transcription factor code. Cell 113:73–86.

Anderson KV, Lengyel JA (1979) Rates of synthesis of major classes of RNA in *Drosophila* embryos. Dev Biol 70:217–231.

Boll W, Noll M (2002) The *Drosophila* Pox neuro gene: control of male courtship behavior and fertility as revealed by a complete dissection of all enhancers. Development 129:5667–5681.

Brand AH, Perrimon N (1993) Targeted gene expression as a means of altering cell fates and generating dominant phenotypes. Development 118:401–415.

Caesar S, Greiner M, Schlenstedt G (2006) Kap120 functions as a nuclear import receptor for ribosome assembly factor Rpf1 in yeast. Mol Cell Biol 26:3170–3180.

Chan CC, Zhang S, Rousset R, Wharton KA (2008) *Drosophila* Naked cuticle (Nkd) engages the nuclear import adaptor Importin-alpha3 to antagonize Wnt/beta-catenin signaling. Dev Biol 318:17–28.

Chou TB, Perrimon N (1992) Use of a yeast site-specific recombinase to produce female germline chimeras in *Drosophila*. Genetics 131:643–653.

Chou TB, Perrimon N (1996) The autosomal FLP-DFS technique for generating germline mosaics in *Drosophila* melanogaster. Genetics 144:1673–1679.

Collins CA, DiAntonio A (2007) Synaptic development: insights from *Drosophila*. Curr Opin Neurobiol 17:35–42.

Collins CA, Wairkar YP, Johnson SL, DiAntonio A (2006) Highwire restrains synaptic growth by attenuating a MAP kinase signal. Neuron 51:57–69.

Coombe PE (1986) The large monopolar cells L1 and L2 are responsible for ERG transients in *Drosophila*. J Comp Physiol A Neuroethol Sens Neural Behav Physiol 159:655–665.

Davis BN, Hilyard AC, Lagna G, Hata A (2008) SMAD proteins control DROSHA-mediated microRNA maturation. Nature 454:56–61.

Deitcher DL, Ueda A, Stewart BA, Burgess RW, Kidokoro Y, Schwarz TL (1998) Distinct requirements for evoked and spontaneous release of neurotransmitter are revealed by mutations in the *Drosophila* gene neuronal-synaptobrevin. J Neurosci 18:2028–2039.

DiAntonio A, Parfitt KD, Schwarz TL (1993) Synaptic transmission persists in synaptotagmin mutants of *Drosophila*. Cell 73:1281–1290.

DiAntonio A, Petersen SA, Heckmann M, Goodman CS (1999) Glutamate receptor expression regulates quantal size and quantal content at the *Drosophila* neuromuscular junction. J Neurosci 19:3023–3032.

Dickman D, Horne JA, Meinertzhagen IA, Schwarz TL (2005) A slowed classical pathway rather than kiss-and-run mediates endocytosis at synapses lacking synaptojanin and endophilin. Cell 123:521–533.

Dickman D, Kurshan P, Schwarz TL (2008) Mutations in a *Drosophila* $\alpha_2$delta voltage-gated calcium channel subunit reveal a crucial synaptic function. J Neurosci 28:31–38.

Dudu V, Bittig T, Entchev E, Kicheva A, Julicher F, Gonzalez-Gaitan M (2006) Postsynaptic mad signaling at the *Drosophila* neuromuscular junction. Curr Biol 16:625–635.

Duncan JE, Warrior R (2002) The cytoplasmic dynein and kinesin motors have interdependent roles in patterning the *Drosophila* oocyte. Curr Biol 12:1982–1991.

Eaton BA, Fetter RD, Davis GW (2002) Dynactin is necessary for synapse stabilization. Neuron 34:729–741.

Fabian-Fine R, Verstreken P, Hiesinger PR, Horne JA, Kostyleva R, Zhou Y, Bellen HJ, Meinertzhagen IA (2003) Endophilin promotes a late step in endocytosis at glial invaginations in *Drosophila* photoreceptor terminals. J Neurosci 23:10732–10744.

Finlay DR, Newmeyer DD, Price TM, Forbes DJ (1987) Inhibition of *in vitro* nuclear transport by a lectin that binds to nuclear pores. J Cell Biol 104:189–200.

Frank CA, Kennedy MJ, Goold CP, Marek KW, Davis GW (2006) Mechanisms underlying the rapid induction and sustained expression of synaptic homeostasis. Neuron 52:663–677.

Fried H, Kutay U (2003) Nucleocytoplasmic transport: taking an inventory. Cell Mol Life Sci 60:1659–1688.

Giagtzoglou N, Lin YQ, Haueter C, Bellen HJ (2009) Importin 13 regulates

neurotransmitter release at the *Drosophila* neuromuscular junction. J Neurosci 29:5628–5639.
Goodman CS, Shatz CJ (1993) Developmental mechanisms that generate precise patterns of neuronal connectivity. Cell [Suppl] 72:77–98.
Goold CP, Davis GW (2007) The BMP ligand Gbb gates the expression of synaptic homeostasis independent of synaptic growth control. Neuron 56:109–123.
Görlich D, Kutay U (1999) Transport between the cell nucleus and the cytoplasm. Annu Rev Cell Dev Biol 15:607–660.
Görlich D, Kostka S, Kraft R, Dingwall C, Laskey RA, Hartmann E, Prehn S (1995) Two different subunits of importin cooperate to recognize nuclear localization signals and bind them to the nuclear envelope. Curr Biol 5:383–392.
Greer PL, Greenberg ME (2008) From synapse to nucleus: calcium-dependent gene transcription in the control of synapse development and function. Neuron 59:846–860.
Guillemain G, Muñoz-Alonso MJ, Cassany A, Loizeau M, Faussat AM, Burnol AF, Leturque A (2002) Karyopherin alpha2: a control step of glucose-sensitive gene expression in hepatic cells. Biochem J 364:201–209.
Haerry TE, Khalsa O, O'Connor MB, Wharton KA (1998) Synergistic signaling by two BMP ligands through the SAX and TKV receptors controls wing growth and patterning in *Drosophila*. Development 125:3977–3987.
Hanz S, Perlson E, Willis D, Zheng JQ, Massarwa R, Huerta JJ, Koltzenburg M, Kohler M, van-Minnen J, Twiss JL, Fainzilber M (2003) Axoplasmic importins enable retrograde injury signaling in lesioned nerve. Neuron 40:1095–1104.
Harel A, Forbes DJ (2004) Importin beta: conducting a much larger cellular symphony. Mol Cell 16:319–330.
Harlow E, Lane D (1988) Antibodies: a laboratory manual. Cold Spring Harbor, NY: Cold Spring Harbor Laboratory.
Hazelett DJ, Bourouis M, Walldorf U, Treisman JE (1998) decapentaplegic and wingless are regulated by eyes absent and eyegone and interact to direct the pattern of retinal differentiation in the eye disc. Development 125:3741–3751.
Heisenberg M (1971) Separation of receptor and lamina potentials in the electroretinogram of normal and mutant *Drosophila*. J Exp Biol 55:85–100.
Hiesinger PR, Zhai RG, Zhou Y, Koh TW, Mehta SQ, Schulze KL, Cao Y, Verstreken P, Clandinin TR, Fischbach KF, Meinertzhagen IA, Bellen HJ (2006) Activity-independent prespecification of synaptic partners in the visual map of *Drosophila*. Curr Biol 16:1835–1843.
Hoang B, Chiba A (2001) Single-cell analysis of *Drosophila* larval neuromuscular synapses. Dev Biol 229:55–70.
Hofbauer A, Ebel T, Waltenspiel B, Oswald P, Chen YC, Halder P, Biskup S, Lewandrowski U, Winkler C, Sickmann A, Buchner S, Buchner E (2009) The Wuerzburg hybridoma library against *Drosophila* brain. J Neurogenet 23:78–91.
Holley SA, Neul JL, Attisano L, Wrana JL, Sasai Y, O'Connor MB, De Robertis EM, Ferguson EL (1996) The *Xenopus* dorsalizing factor noggin ventralizes *Drosophila* embryos by preventing DPP from activating its receptor. Cell 86:607–617.
Hoodless PA, Haerry T, Abdollah S, Stapleton M, O'Connor MB, Attisano L, Wrana JL (1996) MADR1, a MAD-related protein that functions in BMP2 signaling pathways. Cell 85:489–500.
Hoover LL, Kubalak SW (2008) Holding their own: the noncanonical roles of Smad proteins. Sci Signal 1:pe48.
Hummel T, Krukkert K, Roos J, Davis G, Klämbt C (2000) *Drosophila* Futsch/22C10 is a MAP1B-like protein required for dendritic and axonal development. Neuron 26:357–370.
Jakel S, Mingot JM, Schwarzmaier P, Hartmann E, Gorlich D (2002) Importins fulfill a dual function as nuclear import receptors and cytoplasmic chaperones for exposed basic domains. EMBO J 21:377–386.
James BP, Bunch TA, Krishnamoorthy S, Perkins LA, Brower DL (2007) Nuclear localization of the ERK MAP kinase mediated by *Drosophila* alphaPS2betaPS integrin and importin-7. Mol Biol Cell 18:4190–4199.
Johansen J, Halpern ME, Johansen KM, Keshishian H (1989) Stereotypic morphology of glutamatergic synapses on identified muscle cells of *Drosophila* larvae. J Neurosci 9:710–725.
Kelly LE (1983) The regulation of phosphorylation of a specific protein in synaptosomal fractions from *Drosophila* heads: the effects of light and two visual mutants. Cell Mol Neurobiol 3:127–141.
Keshishian H, Kim YS (2004) Orchestrating development and function: retrograde BMP signaling in the *Drosophila* nervous system. Trends Neurosci 27:143–147.
Keshishian H, Broadie K, Chiba A, Bate M (1996) The *drosophila* neuromuscular junction: a model system for studying synaptic development and function. Annu Rev Neurosci 19:545–575.
Kittel RJ, Wichmann C, Rasse TM, Fouquet W, Schmidt M, Schmid A, Wagh DA, Pawlu C, Kellner RR, Willig KI, Hell SW, Buchner E, Heckmann M, Sigrist SJ (2006) Bruchpilot promotes active zone assembly, Ca^{2+} channel clustering, and vesicle release. Science 312:1051–1054.
Laemmli UK (1970) Cleavage of structural proteins during the assembly of the head of bacteriophage T4. Nature 227:680–685.
Lai KO, Zhao Y, Ch'ng TH, Martin KC (2008) Importin-mediated retrograde transport of CREB2 from distal processes to the nucleus in neurons. Proc Natl Acad Sci U S A 105:17175–17180.
Lee T, Luo L (1999) Mosaic analysis with a repressible cell marker for studies of gene function in neuronal morphogenesis. Neuron 22:451–461.
Li J, Li WX (2006) A novel function of *Drosophila* eIF4A as a negative regulator of Dpp/BMP signalling that mediates SMAD degradation. Nat Cell Biol 8:1407–1414.
Lnenicka GA, Keshishian H (2000) Identified motor terminals in *Drosophila* larvae show distinct differences in morphology and physiology. J Neurobiol 43:186–197.
Luo L, Liao Y, Jan LY, Jan YN (1994) Distinct morphogenetic functions of similar small GTPases: *Drosophila* Drac1 is involved in axonal outgrowth and myoblast fusion. Genes Dev 8:1787–1802.
Mackler JM, Drummond JA, Loewen CA, Robinson IM, Reist NE (2002) The C(2)B Ca(2+)-binding motif of synaptotagmin is required for synaptic transmission *in vivo*. Nature 418:340–344.
Marqués G (2005) Morphogens and synaptogenesis in *Drosophila*. J Neurobiol 64:417–434.
Marqués G, Bao H, Haerry TE, Shimell MJ, Duchek P, Zhang B, O'Connor MB (2002) The *Drosophila* BMP type II receptor Wishful Thinking regulates neuromuscular synapse morphology and function. Neuron 33:529–543.
Marqués G, Haerry TE, Crotty ML, Xue M, Zhang B, O'Connor MB (2003) Retrograde Gbb signaling through the Bmp type 2 receptor wishful thinking regulates systemic FMRFa expression in *Drosophila*. Development 130:5457–5470.
Marrus SB, DiAntonio A (2004) Preferential localization of glutamate receptors opposite sites of high presynaptic release. Curr Biol 14:924–931.
Marrus SB, Portman SL, Allen MJ, Moffat KG, DiAntonio A (2004) Differential localization of glutamate receptor subunits at the *Drosophila* neuromuscular junction. J Neurosci 24:1406–1415.
Martin AR (1955) A further study of the statistical composition on the end-plate potential. J Physiol 130:114–122.
McCabe BD, Marqués G, Haghighi AP, Fetter RD, Crotty ML, Haerry TE, Goodman CS, O'Connor MB (2003) The BMP homolog Gbb provides a retrograde signal that regulates synaptic growth at the *Drosophila* neuromuscular junction. Neuron 39:241–254.
McCabe BD, Hom S, Aberle H, Fetter RD, Marqués G, Haerry TE, Wan H, O'Connor MB, Goodman CS, Haghighi AP (2004) Highwire regulates presynaptic BMP signaling essential for synaptic growth. Neuron 41:891–905.
Meinertzhagen IA (1996) Ultrastructure and quantification of synapses in the insect nervous system. J Neurosci Methods 69:59–73.
Melkonian KA, Maier KC, Godfrey JE, Rodgers M, Schroer TA (2007) Mechanism of dynamitin-mediated disruption of dynactin. J Biol Chem 282:19355–19364.
Merino C, Penney J, Gonzalez M, Tsurudome K, Moujahidine M, O'Connor MB, Verheyen EM, Haghighi P (2009) Nemo kinase interacts with Mad to coordinate synaptic growth at the *Drosophila* neuromuscular junction. J Cell Biol 185:713–725.
Moroianu J, Hijikata M, Blobel G, Radu A (1995) Mammalian karyopherin alpha 1 beta and alpha 2 beta heterodimers: alpha 1 or alpha 2 subunit binds nuclear localization signal and beta subunit interacts with peptide repeat-containing nucleoporins. Proc Natl Acad Sci U S A 92:6532–6536.
Mosammaparast N, Pemberton L (2004) Karyopherins: from nuclear-transport mediators to nuclear-function regulators. Trends Cell Biol 14:547–556.
Murthy M, Ranjan R, Denef N, Higashi ME, Schupbach T, Schwarz TL (2005) Sec6 mutations and the *Drosophila* exocyst complex. J Cell Sci 118:1139–1150.

Nellen D, Burke R, Struhl G, Basler K (1996) Direct and long-range action of a DPP morphogen gradient. Cell 85:357–368.

O'Connor-Giles KM, Ho LL, Ganetzky B (2008) Nervous wreck interacts with thickveins and the endocytic machinery to attenuate retrograde BMP signaling during synaptic growth. Neuron 58:507–518.

Otis KO, Thompson KR, Martin KC (2006) Importin-mediated nuclear transport in neurons. Curr Opin Neurobiol 16:329–335.

Pack-Chung E, Kurshan P, Dickman D, Schwarz TL (2007) A *Drosophila* kinesin required for synaptic bouton formation and synaptic vesicle transport. Nat Neurosci 10:980–989.

Paine PL, Moore LC, Horowitz SB (1975) Nuclear envelope permeability. Nature 254:109–114.

Perlson E, Hanz S, Ben-Yaakov K, Segal-Ruder Y, Seger R, Fainzilber M (2005) Vimentin-dependent spatial translocation of an activated MAP kinase in injured nerve. Neuron 45:715–726.

Perry RB, Fainzilber M (2009) Nuclear transport factors in neuronal function. Semin Cell Dev Biol 20:600–606.

Persson U, Izumi H, Souchelnytskyi S, Itoh S, Grimsby S, Engstrom U, Heldin CH, Funa K, ten Dijke P (1998) The L45 loop in type I receptors for TGF-beta family members is a critical determinant in specifying Smad isoform activation. FEBS Lett 434:83–87.

Peters R (1983) Nuclear envelope permeability measured by fluorescence microphotolysis of single liver cell nuclei. J Biol Chem 258:11427–11429.

Petersen SA, Fetter RD, Noordermeer JN, Goodman CS, DiAntonio A (1997) Genetic analysis of glutamate receptors in *Drosophila* reveals a retrograde signal regulating presynaptic transmitter release. Neuron 19:1237–1248.

Plafker SM, Macara IG (2000) Importin-11, a nuclear import receptor for the ubiquitin-conjugating enzyme, UbcM2. EMBO J 19:5502–5513.

Plafker SM, Macara IG (2002) Ribosomal protein L12 uses a distinct nuclear import pathway mediated by importin 11. Mol Cell Biol 22:1266–1275.

Plafker SM, Plafker KS, Weissman AM, Macara IG (2004) Ubiquitin charging of human class III ubiquitin-conjugating enzymes triggers their nuclear import. J Cell Biol 167:649–659.

Rexach M, Blobel G (1995) Protein import into nuclei: association and dissociation reactions involving transport substrate, transport factors, and nucleoporins. Cell 83:683–692.

Riemer D, Stuurman N, Berrios M, Hunter C, Fisher PA, Weber K (1995) Expression of *Drosophila* lamin C is developmentally regulated: analogies with vertebrate A-type lamins. J Cell Sci 108:3189–3198.

Roos J, Hummel T, Ng N, Klämbt C, Davis GW (2000) *Drosophila* Futsch regulates synaptic microtubule organization and is necessary for synaptic growth. Neuron 26:371–382.

Rubin GM, Spradling AC (1982) Genetic transformation of *Drosophila* with transposable element vectors. Science 218:348–353.

Schuster CM, Davis GW, Fetter RD, Goodman CS (1996) Genetic dissection of structural and functional components of synaptic plasticity. I. Fasciclin II controls synaptic stabilization and growth. Neuron 17:641–654.

Schwarz TL (2006) Transmitter release at the neuromuscular junction. Int Rev Neurobiol 75:105–144.

Sekelsky JJ, Newfeld SJ, Raftery LA, Chartoff EH, Gelbart WM (1995) Genetic characterization and cloning of mothers against dpp, a gene required for decapentaplegic function in *Drosophila* melanogaster. Genetics 139:1347–1358.

Speese SD, Budnik V (2007) Wnts: up-and-coming at the synapse. Trends Neurosci 30:268–275.

Stewart BA, Atwood HL, Renger JJ, Wang J, Wu CF (1994) Improved stability of *Drosophila* larval neuromuscular preparations in haemolymph-like physiological solutions. J Comp Physiol A Neuroethol Sens Neural Behav Physiol 175:179–191.

Stowers RS, Schwarz TL (1999) A genetic method for generating *Drosophila* eyes composed exclusively of mitotic clones of a single genotype. Genetics 152:1631–1639.

Stowers RS, Megeath LJ, Gorska-Andrzejak J, Meinertzhagen IA, Schwarz TL (2002) Axonal transport of mitochondria to synapses depends on milton, a novel *Drosophila* protein. Neuron 36:1063–1077.

Tang Y, Liu Z, Zhao L, Clemens TL, Cao X (2008) Smad7 stabilizes beta-catenin binding to E-cadherin complex and promotes cell-cell adhesion. J Biol Chem 283:23956–23963.

Thompson KR, Otis KO, Chen DY, Zhao Y, O'Dell TJ, Martin KC (2004) Synapse to nucleus signaling during long-term synaptic plasticity; a role for the classical active nuclear import pathway. Neuron 44:997–1009.

Ting CY, Herman T, Yonekura S, Gao S, Wang J, Serpe M, O'Connor MB, Zipursky SL, Lee CH (2007) Tiling of r7 axons in the *Drosophila* visual system is mediated both by transduction of an activin signal to the nucleus and by mutual repulsion. Neuron 56:793–806.

von Bubnoff A, Cho KW (2001) Intracellular BMP signaling regulation in vertebrates: pathway or network? Dev Biol 239:1–14.

Vrailas AD, Marenda DR, Cook SE, Powers MA, Lorenzen JA, Perkins LA, Moses K (2006) smoothened and thickveins regulate Moleskin/Importin 7-mediated MAP kinase signaling in the developing *Drosophila* eye. Development 133:1485–1494.

Wagh D, Rasse TM, Asan E, Hofbauer A, Schwenkert I, Durrbeck H, Buchner S, Dabauvalle M, Schmidt M, Qin G (2006) Bruchpilot, a protein with homology to ELKS/CAST, is required for structural integrity and function of synaptic active zones in *Drosophila*. Neuron 49:833–844.

Wang X, Shaw W, Tsang H, Reid E, O'Kane C (2007) *Drosophila* spichthyin inhibits BMP signaling and regulates synaptic growth and axonal microtubules. Nat Neurosci 10:177–185.

Wharton KA, Cook JM, Torres-Schumann S, de Castro K, Borod E, Phillips DA (1999) Genetic analysis of the bone morphogenetic protein-related gene, gbb, identifies multiple requirements during *Drosophila* development. Genetics 152:629–640.

Wodarz A, Hinz U, Engelbert M, Knust E (1995) Expression of crumbs confers apical character on plasma membrane domains of ectodermal epithelia of *Drosophila*. Cell 82:67–76.

Xu L, Yao X, Chen X, Lu P, Zhang B, Ip YT (2007) Msk is required for nuclear import of TGF-{beta}/BMP-activated Smads. J Cell Biol 178:981–994.

Xu T, Rubin GM (1993) Analysis of genetic mosaics in developing and adult *Drosophila* tissues. Development 117:1223–1237.

Zhu H, Kavsak P, Abdollah S, Wrana JL, Thomsen GH (1999) A SMAD ubiquitin ligase targets the BMP pathway and affects embryonic pattern formation. Nature 400:687–693.